Title:

Autoimmune antibody-induced neuronal hyperactivity triggers pathological Tau in IgLON5 disease

Authors:

Bilge Askin[1,2], César Cordero Gómez[1,3], Sophie Lan-Linh Duong[1,3,4], Cagla Kilic[1], Alexander Goihl[5], Andrew Newman[6], Jessica Wagner[7,8,9], Valentine Thomas[1], Janne Lamberty[1], Sabrina Huebschmann[1], Ekaterina Semenova[1], Peter Körtvelyessy[3,10], Dirk Reinhold[5], Hans-Christian Kornau[1,11], Paul Turko[12], Jonas J. Neher[7,8,9], Dietmar Schmitz[1,2,11], Benjamin R. Rost[1], Lisa Diez[1], Harald Prüss[1,2,3], Susanne Wegmann[1,2]*

Affiliations:

[1] German Center for Neurodegenerative Diseases (DZNE), Berlin, Germany
[2] Einstein Center for Neurosciences (ECN), Charité - Universitätsmedizin Berlin, Berlin, Germany
[3] Department of Neurology and Experimental Neurology, Charité – Universitätsmedizin Berlin, Berlin, Germany
[4] Berlin Institute of Health (BIH) at Charité – Universitätsmedizin Berlin, Berlin, Germany
[5] Institute of Molecular and Clinical Immunology, Otto-von-Guericke-University, Magdeburg, Germany
[6] Institute of Cell Biology and Neurobiology, Charité– Universitätsmedizin Berlin, Berlin, Germany
[7] German Center for Neurodegenerative Diseases (DZNE), Munich, Germany
[8] Metabolic Biochemistry, Biomedical Center Munich (BMC), Faculty of Medicine, LMU Munich, Germany
[9] Munich Cluster for Systems Neurology (SyNergy), Munich, Germany
[10] German Center for Neurodegenerative Diseases (DZNE), Magdeburg, Germany
[11] Neuroscience Research Center (NWFZ), Charité-Universitätsmedizin Berlin, Germany
[12] Institute of Integrative Neuroanatomy, Charité, Berlin, Germany

* corresponding author: susanne.wegmann@dzne.de

Key words:

Anti-IgLON5 disease, autoantibodies, autoimmune encephalitis, tauopathy, Tau, hyperactivity, neurodegeneration, neuroinflammation

Abbreviations:

AABs - Autoantibodies
AD - Alzheimer's disease
AE - Autoimmune encephalitis
AMPA -α-amino-3-hydroxy-5-methyl-4-isoxazolepropionic acid
Aβ - Amyloid-beta
BSA - Bovine serum albumin
CA1- Hippocampal area CA1

43 Ca^{2+} - Calcium
44 CA3 - Hippocampal area CA3
45 CSF - Cerebrospinal fluid
46 DG - Dentate gyrus
47 ELISA - Enzyme-Linked Immunosorbent Assay
48 EPSC - Excitatory postsynaptic current
49 FTD - Frontotemporal dementia
50 GFAP - Glial fibrillary acidic protein
51 GO - Gene ontology
52 hNSCs - Human neural stem cells
53 IF - Immunofluorescence
54 Ig - Immunoglobulin
55 IHC - Immunohistochemistry
56 KEGG - Kyoto encyclopedia of genes and genomes
57 LDH - Lactate dehydrogenase
58 LGI1 - Leucine-rich glioma-inactivated 1 protein
59 mCtrl - Human monoclonal, non-reactive IgG
60 MF - Mossy fiber
61 MFG-E8 - Milk fat globule epidermal growth factor 8
62 NBA - Neurobasal-A
63 NfL - Neurofilament light chain
64 NGS - Normal goat serum
65 NMDA - N-methyl-D-aspartate
66 p-Tau - Phosphorylated Tau
67 PBS - Phosphate-buffered saline
68 PBS-T - PBS containing Tween
69 pCtrl - Human serum-derived control IgG purified from healthy control serum in-house
70 $pCtrl_{rec}$ - Commercial normal human IgG
71 PFA - Paraformaldehyde
72 PLL - Poly-L-lysine
73 PPR - Paired-pulse ratios
74 Pvr - Synaptic vesicle fusion
75 RT - Room temperature
76 SP - Signal peptide SP
77 TBS - Tris-buffered saline
78

79 **Abstract**

80 Anti-IgLON5 disease is an autoimmunity/neurodegeneration overlap disorder in which
81 autoantibodies (AABs) against the neuronal cell surface protein IgLON5 lead to profound brain
82 dysfunction. Brains of patients show Tau pathology, neuroinflammation, and
83 neurodegeneration in multiple brain regions. Through administering patient-derived α-IgLON5
84 AABs to mice and cultured neurons, we here deciphered the cellular mechanisms of Tau
85 pathology and neurodegeneration in α-IgLON5 disease, highlighting a central role of neuronal
86 activity modulation in the disease pathology. Pathogenic human α-IgLON5 AABs induced
87 acute neuronal hyperactivity, which triggered Tau changes typically found early in Tau-related
88 neurodegenerative diseases like Alzheimer's disease (AD). α-IgLON5 AAB-induced Tau

phosphorylation and somatodendritic resorting selectively occurred in key hippocampal connections, involving dentate gyrus granule cells, mossy fiber projections and commissural fiber tracts. These changes were accompanied by a Tau-specific neuroinflammatory response, involving the complement pathway, microglial MHC class II proteins, T cell receptors, and deregulation of synaptic activity and cell-cell interactions. These findings provide new insights into the origin of autoimmune-triggered α-IgLON5 disease pathology and highlight that, similar to recent reports in AD patients, neuronal hyperactivity may be a disease-overarching driver of Tau pathology.

Introduction

Autoimmune antibodies (autoantibodies, AABs) directed against neuronal or glial epitopes in the brain can cause neuropathological conditions or exacerbate existing diseases [1]. The trigger for the production of AABs against brain epitopes is not fully understood, but abnormal immune responses due to genetic predispositions, viral infections, or tumors can contribute to certain autoimmune encephalitis (AE) cases [2].

α-IgLON5 disease is a recently described, rare but severe neurological disorder characterized by the presence of AABs targeting the neuronal cell surface protein IgLON5 [3]. Individuals diagnosed with α-IgLON5 disease demonstrate diverse clinical manifestations and commonly experience sleep behavior abnormalities, movement disorders, memory deficits, and seizures [4–6]. Brains of α-IgLON5 patients show intraneuronal accumulations of highly phosphorylated Tau protein (p-Tau) in several regions, including hippocampus, cerebellum, brain stem, hypothalamus, and basal ganglia, as well as in the spinal cord [3,7]. Pathological hallmarks in primary and secondary tauopathies, such as frontotemporal dementia (FTD) variants and Alzheimer's disease (AD), include high phosphorylation, somatodendritic re-sorting, aggregation and deposition of the microtubule associated protein Tau [8,9]. Although α-IgLON5 disease differs from other tauopathies because of its unique set of clinical manifestations, anatomical Tau distribution, and its autoimmune context, it can be categorized as a novel tauopathy due to the histological similarities to well-known diseases with Tau pathology [3].

The discovery of α-IgLON5 disease poses the fundamental questions of whether and how AABs against a cell surface protein can trigger intracellular Tau aggregation and associated pathological changes in the brain. Understanding the mechanisms of how autoimmunity can induce neurodegeneration could not only lead to specific treatment options for α-IgLON5 and

122 further autoantibody-mediated brain diseases, but also provide important insights into how
123 and why pathological Tau changes occur in more than 20 different neurological diseases [10].

124 The IgLON protein family is a group of immunoglobulin (Ig) domain cell adhesion molecules
125 comprising five gene members (OPCML (=IgLON1), NTM (=IgLON2), LSAMP (=IgLON3),
126 NEGR1 (=IgLON4), and IgLON5) [11]. IgLON5 is a GPI-anchored surface protein with three Ig-
127 domains (Ig1, Ig2 and Ig3) that extend into the extracellular space and mediate homo-dimer
128 and hetero-dimer formation with other IgLON family members on the cell surface and at the
129 synaptic cleft [12–14]. In humans and mice, IgLON5 is primarily expressed in neuronal cells in the
130 brain, including the hippocampal formation, cortex, hypothalamus, brain stem, basal ganglia,
131 cerebellum and spinal cord (The Human Protein Atlas:
132 https://www.proteinatlas.org/ENSG00000142549-IGLON5; Expression atlas:
133 https://www.ebi.ac.uk/gxa/home). The physiological function of IgLON5 is not fully understood,
134 however, other IgLON family members have been implicated in neuronal cell adhesion, neurite
135 growth, neural circuit and synapse formation [15–17].

136 A neurotoxic potential of α-IgLON5 AABs was previously suggested based on the observation
137 that long-term treatment (1-4 weeks) of cultured neurons with α-IgLON5 AABs induces
138 common neurodegenerative phenotypes, such as Tau phosphorylation, cytoskeleton
139 disruption [18], synapse loss, and cell death [19]. Here, using *in vitro* and *in vivo* models, we now
140 unravelled the origin of these changes through demonstrating that α-IgLON5 AABs trigger
141 acute neuronal hyperactivity, which activates persistent neuronal Tau phosphorylation and
142 somatodendritic resorting. These changes occur in selected hippocampal connections,
143 including mossy fiber (MF) connections between dentate gyrus (DG) and hippocampal region
144 CA3, and projections onto ventral CA1, and are accompanied by distinct gene expression
145 signatures indicative of neuroinflammation and synaptic restructuring/activity modulation.
146 These findings elucidate the cellular mechanism by which α-IgLON5 AABs trigger tauopathy-
147 like pathology and neurotoxicity in α-IgLON5 disease, and thereby provide the foundation for
148 the development of novel α-IgLON5 disease treatment approaches. In addition, our data
149 demonstrate that neuronal hyperexcitability is sufficient to drive Tau pathology and may
150 therefore represent a central pathomechanism across different neurological diseases
151 exhibiting Tau pathology.

152

153 # Results

154 ***Case study and isolation of high-affinity α-IgLON5 AABs from α-IgLON5 patient plasma***

155 A 59-year-old male patient presented with a history of sleep apnea, myoclonic jerks,
156 dysarthria, and gait disorder for one year. After ruling out common neurodegenerative
157 diseases by clinical expertise, we detected α-IgLON5 AABs both in cerebrospinal fluid (CSF;
158 at a titer of 1:100) and serum (at a. titer of 1:1000) of the patient, confirming a diagnosis of α-
159 IgLON5 disease. Oral treatment with the corticosteroid immunosuppressant
160 Methylprednisolone did not improve the symptoms. This treatment approach was followed by
161 plasmapheresis to remove AABs from the serum, after which the patient was stable with the
162 application of non-invasive ventilation at night and immunosuppressive therapy (improved
163 sleep apnea and frequency of the myoclonic jerks; remission was not achieved).
164 To isolate α-IgLON5 AABs from the patient's plasma for fine characterization, recombinant
165 human IgLON5-Fc chimera were immobilized on affinity chromatography purification columns
166 (Fig. 1a). The purified α-IgLON5 AABs (heavy chain ~50 kDa), light chain ~25 kDa; Fig. 1b)
167 had a purity of 84±7% (determined based on signal intensity of [heavy + light chain] relative to
168 total signal in SDS-PAGE). In dot blot assays, the α-IgLON5 AABs were reactive to
169 recombinant IgLON5 protein but not to LGI1 (leucine-rich glioma-inactivated 1) protein, which
170 functioned as a control for unspecific binding (Fig. 1c). Furthermore, isolated α-IgLON5 AABs
171 spotted on a dot blot membrane were recognized by α-human IgG secondary antibodies
172 specific for subclasses IgG1, IgG2, IgG3 and IgG4 (Supplemental Fig. S1a), indicating that
173 the presence of a polyclonal pool of α-IgLON5 AABs in the patient's plasma. An antibody pool
174 derived from healthy subject serum (pCtrl), which does not detect IgLON5 and contained all
175 human IgG subclasses, was used as control.
176

177 ***α-IgLON5 AABs bind cell surface IgLON5 protein on human and mouse neurons***

178 To validate the specificity of the isolated patient-derived α-IgLON5 AABs, we expressed full-
179 length human IgLON5 protein (Fig. 1d) in HEK cells and detected the binding of α-IgLON5
180 AABs after incubation with fluorescently labeled α-human secondary IgGs (Fig. 1e). We
181 detected binding to full-length IgLON5 as well as all (combinations of) individual GPI-anchored
182 Ig domains (Ig1/2/3), indicating binding of the isolated polyclonal α-IgLON5 AAB pool to every
183 domain of IgLON5. Titrating the isolated α-IgLON5 AABs to cells recombinantly expressing
184 human IgLON5 showed a dose dependent binding and suggested an EC_{50}=8 μg/ml (K_D=56
185 μM at MW_{AAB}=150 kDa; Fig. 1f); the relative binding strength was determined based on
186 immunofluorescence intensity after fixation and labeling with fluorescently labeled anti-human

187 IgG. Notably, the molecular binding affinity of α-IgLON5 AABs to IgLON5 protein may be far
188 higher when determined in purified preparations. Furthermore, α-IgLON5 AABs also bound to
189 the surface of human neural stem cells (hNSCs) (Fig. 1g). In fresh frozen mouse brain
190 sections, α-IgLON5 AABs showed immunoreactivity across various brain regions, including
191 the cortex, olfactory bulb, hippocampus, mid brain, hind brain (pons, medulla) and cerebellum
192 (Fig. 1h). Notably, binding of α-IgLON5 AABs aligns with IgLON5 expression in these brain
193 regions in mice (Supplemental Fig. S1b).
194 To test whether α-IgLON5 AABs bound preferably to pre- or post-synaptic IgLON5, we treated
195 primary hippocampal mouse neuron cultures with α-IgLON5 AABs and determined the co-
196 localization with MAP2 and pre- (Synapsin-1) and postsynaptic (PSD-95) markers. These
197 experiments suggested no preference of α-IgLON5 AABs for dendritic or axonal processes
198 (Fig. 1i), and similar partial co-localization with pre- and post-synaptic structures (Fig. 1j).
199 Immunolabeling was detectable also with detergent permeabilization, hence representing cell
200 surface IgLON5 labeling.
201 Neurologically active AABs targeting neuronal surface antigens, e.g., LGI1, N-methyl-D-
202 aspartate (NMDA), α-amino-3-hydroxy-5-methyl-4-isoxazolepropionic acid (AMPA) and
203 glycine receptors, can induce antibody-antigen complexes and receptor internalization upon
204 binding, which contributes to AE pathophysiology [2]. Accordingly, we detected the
205 internalization and endo-lysosomal entry of α-IgLON5 AABs (labeled with pHrodo™ Red) in
206 cultured neurons (after 1 day and 2 days) and in cells expressing human IgLON5 (after 4 h),
207 which was less pronounced for a pool of IgGs lacking antibodies against brain cell targets
208 (pCtrl, isolated from healthy control serum; Supplemental Fig. S1e). Previous data indicated
209 that IgG1, but not IgG4 fractions of α-IgLON5 AABs are internalized by neurons [20], suggesting
210 that only a fraction of our α-IgLON5 AABs may be internalized.
211
212 Together these data show that the plasma of the α-IgLON5 patient contains a high affinity
213 polyclonal pool of α-IgLON5 AABs that are reactive to different epitopes in different sub-
214 domains of the IgLON5 protein (Fig. 1k).
215
216 ***Patient-derived α-IgLON5 AABs induce motor deficits in mice***

217 *Postmortem* brains of α-IgLON5 patients are characterized by the intraneuronal deposition of
218 phosphorylated Tau (p-Tau) in various brain regions [3,7]. Like in other tauopathies, the
219 presence of p-Tau appears to correlate with neuroinflammation and neuronal loss in α-IgLON5
220 affected regions.

221 To test whether α-IgLON5 AABs are sufficient to induce these changes in the brain, we
222 administered patient-derived α-IgLON5 AABs into the brain of adult wildtype mice
223 cerebroventricular infusion into the right cerebral ventricle for 14 consecutive days; a total
224 amount of 75 μg AABs were infused (~3 μg/g body weight). A serum-derived pool of IgGs from
225 healthy controls (pCtrl), as well as a non-reactive human monoclonal IgG (mCtrl: mGo53 [21])
226 and PBS, were used as control groups. After 14 days of infusion, blood serum and brains were
227 harvested and analyzed for neuroinflammation and p-Tau accumulation (Fig. 2a). Fluorescent
228 immunolabeling of fixed brain sections showed that the α-IgLON5 AABs diffused from the
229 infused ventricle through the ipsilateral hemisphere, with strong binding to ventral regions
230 (e.g., parts of thalamus, hypothalamus, amygdala), and to some extent into the contralateral
231 hippocampus (Fig. 2b; Supplementary Fig. S2a). Animals treated with pCtrl showed far less
232 labeling. These results indicated that patient-polyclonal α-IgLON5 AAB are specific to their
233 target and can bind to IgLON5 *in vivo*.
234 In addition, animals treated with α-IgLON5 AABs showed phenotypic changes. In particular,
235 compared to all control groups (pCtrl, mCtrl, and PBS), the body weight of α-IgLON5 AAB
236 infused animals stagnated for the first 7 days of treatment, leading to a significantly reduced
237 body weight after 6 to 14 days of treatment (Fig. 2c). Assessment of motor function in the
238 rotarod test showed that α-IgLON5 AAB animals started to perform worse on Day 7 (non-
239 significant) and were significantly impaired in motor function on Day 14 (Fig. 2d).
240 To assess whether the pathological changes observed in α-IgLON5 AAB-treated animals were
241 caused by neurodegeneration, we determined the levels of neurofilament light chain (NfL;
242 indicator for axonal damage) and glial fibrillar acidic protein (GFAP; indicator for
243 neuroinflammation) in the serum of the animals at Day 14. α-IgLON5 animals had enhanced
244 serum NfL levels compared to all controls (Fig. 2e left), although this did not reach statistical
245 significance. No difference was detected in GFAP serum levels (Fig. 2e, right). Of note, our
246 measurements of NfL and GFAP levels in serum may lack the sensitivity achieved by
247 measuring their CSF levels, for which increased NfL was previously reported in α-IgLON5
248 patients [18].
249 We also performed staining for milk fat globule epidermal growth factor 8 (MFG-E8), an
250 opsonin for apoptotic cells that recognizes phosphatidylserine exposure (early marker of
251 apoptotic death), which increases with glial activation in mice with amyloid-beta (Aβ)
252 aggregation [22] and upon neuronal Tau aggregation *in vitro* [23]. Although some MFG-E8 staining
253 was evident in all groups, its levels were not affected by AAB treatment (Supplementary Fig.
254 S2b), suggesting that acute administration of AABs did not induce neuronal death at the
255 chosen AAB dose.
256

257 Together these results indicate a high pathogenic potential of the patient-derived α-IgLON5
258 AABs, resulting in an *in vivo* phenotype with in rapid onset of deficits in physical condition
259 (body weight loss) and motor performance of the treated animals.
260

261 ***α-IgLON5 AABs induce neuroinflammation and deregulate neuronal activity related***
262 ***genes***

263 The rather rapid decline of motor function in α-IgLON5 AAB treated animals suggested that
264 α-IgLON5 AABs may have caused cellular and/or molecular changes in the brain directly
265 related to brain function. We tested whether α-IgLON5 AABs induced neuroinflammation,
266 which could explain the rapid onset and progression of symptoms characteristic for different
267 types of AE [1], including α-IgLON5 disease.
268 To this end, we analyzed astrocytosis (GFAP) and microgliosis (Iba1) in brain regions that are
269 affected in α-IgLON5 disease through fluorescence intensity. α-IgLON5 animals showed
270 higher GFAP and Iba1 intensities in several brain regions - including hippocampus,
271 hypothalamus, cerebellum, medial habenula, and periaqueductal gray - compared to PBS and
272 mCtrl treated-animals (Fig. 3a-d; Supplementary Fig. S2c, d). pCtrl but not mCtrl infusion also
273 led to increased GFAP and Iba1 immunoreactivity in some brain areas, particularly in cortex
274 and hypothalamus. This indicated that infusion of polyclonal human antibodies *per se* can
275 trigger an inflammatory response in mice. Nevertheless, α-IgLON5 AABs seemed to
276 additionally cause pathogenic effects, particularly in regions with high IgLON5 protein
277 expression such as the hippocampus.
278 The impaired motor function observed in α-IgLON5 AAB treated animals (Fig. 2d) could be
279 caused by inflammation or other pathological changes in the spinal cord. We therefore
280 investigated glia cell levels in spinal cord gray matter by immunofluorescence, however, we
281 did not find a difference between treatment groups (Supplementary Fig. S2e, f).
282 Notably, in a test cohort that received a higher AAB dose (total amount of 200 μg AAB; 8 μg/g
283 body weight), we also observed weight loss, motor impairments (rotarod at Day 14), and
284 increased microglia (Iba1) and astrocyte (GFAP) activation in brain and spinal cord, which
285 were, however, similar in both α-IgLON5 AAB and pCtrl-infused animals (Supplementary Fig.
286 S4). This suggested that higher doses of patient-derived AABs are *per se* toxic when
287 administered into mice.
288

289 To further resolve molecular changes induced by α-IgLON5 AABs vs. pCtrl, we performed
290 bulk RNAseq. To this end, we used contralateral cortices animals since cells in ipsilateral
291 cortices are compromised by the surgery. α-IgLON5 treated animals had several genes that

292 were significantly up- or downregulated compared to pCtrl animals: genes associated with
293 neuroinflammatory response (e.g., *CXCL10, CXCL16, CCL3, C3,* and *GFAP*) were up-
294 regulated, whereas genes for ion channels (e.g., *SLC10A4, KCNA5,* and *SCN5A*), the
295 dopaminergic system (e.g., *DRD1, DRD2,* and *PPP1R1B*), and cell-cell junction proteins and
296 surface receptors (*NEXN*, *PDLIM3, NTRK1*, and *TACR1*) were down-regulated (Fig. 3e-g;
297 Supplementary Fig. S3; Supplementary Table T1). We confirmed the upregulation of certain
298 neuroinflammation-associated genes on the protein level by immunostaining (Fig. 3h).
299 Interestingly, MHC class II proteins (*CD74, H2-Aa H2-Eb1* and *H2-Ab1*) and CD8 receptor
300 activity related genes (*CD274* and *CCL5*) were also upregulated in α-IgLON5 animals.
301 Immunostaining of hippocampal sections confirmed a small number of CD8-positive (CD8+)
302 T cells in the hippocampus of α-IgLON5 but not pCtrl infused mice. Infiltration of CD8+ T cells
303 was previously suggested to be triggered by Tau pathology and to mediate neurotoxicity in
304 human Tau transgenic mice [24]. Therefore, α-IgLON5 AABs may trigger a similar Tau related
305 pathological cascade.
306
307 Together, these data show that, within 2 weeks, α-IgLON5 AABs induce a distinct pro-
308 inflammatory and neuronal activity-modulating signature in the brain. Additionally, we
309 observed a general glia cell response (increase in Iba1 and GFAP) induced by intrathecal
310 infusion of human autoantibodies (pCtrl and α-IgLON5 AABs) into the mouse.
311
312 ***α-IgLON5 AABs induce Tau phosphorylation in selected hippocampal projections***

313 A characteristic pathological change in the brains of α-IgLON5 patients is the accumulation
314 of p-Tau in the somatodendritic compartment of neurons in the hippocampus and other brain
315 regions [3,7]. However, whether AABs against IgLON5 are directly responsible for Tau changes
316 is not clear. We therefore evaluated whether the cerebroventricular infusion of α-IgLON5
317 AABs into wildtype mice was sufficient to initiate Tau phosphorylation and accumulation in the
318 brain.
319 Western Blot analysis of Tau in lysates from spinal cord, fimbria, and cerebellum suggested
320 no differences in p-Tau between groups (p-Tau pS202/pT205 (AT8), pS396/pS404 (PHF-1),
321 and pT231 (AT180) epitopes); Supplemental Fig. S5a), possibly because the localized p-Tau
322 signal was diluted in bulk tissue analysis.
323 To refine our analysis and detect subtle and spatially restricted changes in Tau
324 phosphorylation, we performed immunofluorescence labeling of p-Tau in brain slices of
325 treated mice. These experiments revealed p-Tau pS396/pS404 (PHF-1) immunoreactivity in
326 the brains of α-IgLON5 AAB but not control (PBS, mCtrl, pCtrl) mice, selectively in (i) cells of
327 the dentate gyrus, (ii) in mossy fiber (MF) projections onto CA3, (iii) in bi-directional projections

328 on ventral CA1 (vCA1) but not dorsal CA1 (dCA1) regions, and (iv) in commissural fibers (CFs)
329 of corpus callosum (CC) (Fig. 4a,b). In other brain regions we did not observe p-Tau
330 pS396/pS404. For p-Tau pS202/pT205 (AT8 epitope), we observed no immunoreactivity in
331 hippocampal brain regions, suggesting that α-IgLON5 AABs may have triggered
332 phosphorylation of selected epitopes on Tau. Comparing the levels of p-Tau pS396/pS404
333 and neuroinflammation in the hippocampus of α-IgLON5 animals, we found a correlation
334 between p-Tau and microglia (Iba1) for α-IgLON5 but not in any of the control groups (Fig. 4c;
335 Supplemental Fig. S5b). No correlation was detected between p-Tau and astrocytes (GFAP).
336 Notably, in the spinal cord (ventral horn), motor neuron cell bodies had more p-Tau
337 pS202/pT205 in α-IgLON5 AAB compared to pCtrl infused mice (not quantified; Supplemental
338 Fig. S5c).
339
340 To better understand the pathogenic potential and cellular mechanism of α-IgLON5 AAB-
341 induced Tau accumulation, we performed experiments in primary hippocampal mouse
342 neurons. Neurons treated with α-IgLON5 AABs for 2 days showed a dose-dependent Tau
343 accumulation in the somatodendritic compartment at 0.1, 1, and 10 μg/ml AABs (Fig. 4d, e),
344 notably in the absence of overt neuronal toxicity or death in the cultures, reflecting our findings
345 *in vivo*. At high concentrations (50 μg/ml), α-IgLON5 AABs induced fragmentation of neuronal
346 processes, indicative of toxicity.
347 The levels of p-Tau (AT8, PHF-1, AT180, pS199 epitopes) in neuronal lysates were similar for
348 α-IgLON5 and Ctrl AAB treated cultures (Supplemental Fig. S5d, e), probably because of a
349 high Tau phosphorylation level in cultured neurons at baseline, which commonly renders
350 Western blot analysis of bulk p-Tau levels in neuronal lysates insensitive to changes.
351 Interestingly, when removing α-IgLON5 AABs after 2 days, the Tau levels in neuronal cell
352 bodies remained similar to conditions of continuous treatment with AABs (Fig. 4f), suggesting
353 that Tau – once activated and resorted – may reside in the somatodendritic compartment for
354 multiple days.
355
356 Together these data show that the infusion of α-IgLON5 AABs for two weeks is sufficient to
357 induce hippocampal glia activation, as well as localized and epitope-specific (pS396/pS404)
358 phosphorylation and dendritic accumulation/resorting of Tau in dentate gyrus granule cells
359 and distinct projections in the hippocampus. These pro-pathological Tau changes may
360 represent the earliest changes occurring in α-IgLON5 disease. Notably, we observed these
361 Tau changes in wildtype mice, which are normally rather resilient to pathological endogenous
362 mouse Tau changes demonstrating the strong pathogenic potential of α-IgLON5 AABs across
363 species.

364 *In vitro*, at doses between 0.1 to 1 μg/ml, patient-derived α-IgLON5 AABs directly triggered
365 prolonged somatodendritic resorting of Tau, a typical reaction in neuronal stress response [25].
366 Higher doses of α-IgLON5 AABs were neurotoxic. These observations suggest that low
367 concentrations of α-IgLON5 AABs could trigger continued stress response and
368 somatodendritic p-Tau resorting in the brains of α-IgLON5 patients.
369

370 ***Acute neuronal hyperactivity drives α-IgLON5 AABs Tau changes***

371 Neuronal hyperactivity, for example during epileptic activity [26], induced by Aβ oligomers [27], or
372 through chemical activity stimulation (e.g., using glutamate [28]) - is a known driver of Tau
373 phosphorylation and somatodendritic resorting. Given that we observed similar Tau changes
374 upon treatment with α-IgLON5 AAB, we asked whether those were linked to neuronal activity
375 as well. IgLON5 has not previously been associated with modulating neuronal excitability.
376 Imaging of spontaneous calcium (Ca^{2+}) transients in GCamp6f expressing hippocampal
377 neurons (DIV13-15; Fig. 5a) treated with a low dose of AABs (0.1 μg/ml) revealed a significant
378 increase in neuronal activity upon exposure to α-IgLON5 compared to control antibodies (Fig.
379 5b-e). This was apparent from an increased average spike rate in cultures treated with α-
380 IgLON5 AABs compared to pCtrl and mCtrl treated cultures after 15 min (average spikes/min
381 at 15 min (mean±SEM): α-IgLON5=5.0±0.1, pCtrl=4.0±0.1, mCtrl=3.2±0.1 spikes/min;
382 N=1095 to 1430 neurons per condition) and after 60 min (average spikes/min: α-
383 Iglon5=5.8±0.1, pCtrl=5.1±0.1, mCtrl=4.8±0.1 spikes/min; N=1199 to 1379 neurons per
384 condition; Fig. 5d). Therefore, the fraction of hyperactive neurons in the cultures increased
385 from ~3% before treatment to ~9% at 15 min and ~11% at 60 min after α-IgLON5 AAB
386 treatment (Fig. 5e; for definition of activity classes see the figure legend). mCtrl and pCtrl
387 treated neurons showed a less pronounced increase of hyperactive neurons (mCtrl: 5% at
388 15min, 7% at 60 min; pCtrl: 7% at 15 min, 7% at 60 min).
389 Notably, this effect was dose-dependent, because at a higher dose of 1 μg/ml AABs, α-
390 IgLON5 AAB treatment induced a drastic increase in neuronal activity (2.6±0.1 spikes/min
391 (mean±SEM), ~50% hyperactive neurons, N=309 neurons) compared to pCtrl (1.9±0.1
392 spikes/min, ~11% hyperactive neurons, N=263 neurons) and untreated control neurons (Fig.
393 5f,g; Supplemental Fig. S6a). After 2 days, we detected mild toxicity in α-IgLON5 AAB treated
394 neurons (LDH assay; Supplemental Fig. S6c) and the average activity dropped again to
395 baseline (=before treatment) (Supplemental Fig. S6b).
396 Next, we wondered whether the reduction in neuronal activity seen after 2 days of α-IgLON5
397 AAB treatment was due to the loss of functional synapses. To this end, we performed
398 electrophysiological recordings in autaptic hippocampal neuron cultures (individual neurons

399 grown on astrocytic micro-islands, forming synapses only with themselves, Supplemental Fig.
400 S6d) treated with AABs (0.1 μg/ml) for 3 days, which showed no difference between treatment
401 groups for all measured parameters (membrane capacitance, resting membrane potential,
402 excitatory postsynaptic current (EPSC) amplitude, EPSC paired-pulse ratio, readily-releasable
403 pool size, synaptic vesicle release probability, EPSC release during 10 Hz stimulation;
404 Supplemental Fig. S6e). That we detected neither a reduction in EPSC amplitude, nor in
405 RRPM size indicated that no synapse loss occurred upon 3 days treatment with α-IgLON5
406 AABs.
407 To test whether α-IgLON5 AAB-induced neuronal activity was the actual trigger for the Tau
408 resorting observed after α-IgLON5 AAB treatment, we removed Ca^{2+} ions from the medium
409 by chelating them with EGTA-AM [29]. This treatment suppressed α-IgLON5 AAB-induced
410 neuronal hyperactivity in a dose dependent manner (Supplementary Fig. S6f-h), and α-
411 IgLON5 AAB-induced somatodendritic Tau re-sorting was no longer observed upon treatment
412 with EGTA-AM (10 μM for 20 min) (Fig. 5h). Therefore, neuronal activity and/or activity induced
413 Ca^{2+} signaling was necessary to activate Tau somatodendritic resorting upon α-IgLON5 AAB
414 exposure.
415 Since we identified neuronal hyperactivity as the driver of Tau resorting induced by α-IgLON5
416 AABs, we hypothesized that other AABs inducing high neuronal activity would induce a similar
417 effect on Tau resorting. To test this idea, we treated neurons with a human monoclonal AAB
418 targeting LGI1 (α-LGI1 AAB), an epilepsy-related protein that regulates excitatory synapses
419 and stabilizes axonal voltage-gated potassium channels [30–32]. We previously showed that α-
420 LGI1 AABs increase cellular excitability and excitatory synaptic transmission of hippocampal
421 CA3 neurons [33]. Here we found that the treatment of neuronal cultures with 1 μg/ml
422 monoclonal α-LGI1 AAB induced Tau resorting similar to α-IgLON5 AABs (Fig. 5i), suggesting
423 that α-LGI1 induced neuronal hyperactivity may also induced Tau activation.
424
425 Together, these observations show that the binding of α-IgLON5 AABs induces acute
426 hyperexcitation (within minutes) that triggers lasting somatodendritic Tau resorting (for days)
427 and a rebalancing of neuronal physiology after transient hyperactivity. When becoming
428 chronic, for example upon extended or repeated exposure of the brain to α-IgLON5 AABs,
429 these adaptations to α-IgLON5 AAB-induced acute hyperexcitation could lead to synaptic loss
430 and neurotoxicity, resulting in a reduction in the overall neuronal network activity (Fig. 5j). In
431 fact, long-term treatment of cultured neurons with α-IgLON5 AABs for multiple weeks has
432 been shown to result in a decrease of synapse numbers [19]. In summary, our data identify acute

433 neuronal hyperactivity as the driver of pro-pathological Tau changes in α-IgLON5 disease –
434 and possibly other AAB-induced neurological conditions.
435

436 Discussion

437 Autoimmune encephalitis (AEs) disorders are characterized by neuroinflammation and
438 neurodegeneration that are induced by AABs targeting brain antigens [2]. AE patients show a
439 range of neurological symptoms, including seizures, psychiatric manifestations, and cognitive
440 deficits. Several AABs against neuronal receptors and cell surface proteins - e.g., NMDA
441 receptors, $GABA_A$ receptors, and LGI1 - lead to AE diseases by altering neuronal physiology
442 and inducing neuroinflammation [1,33–35].

443 Our data now reveal that α-IgLON5 encephalitis – a unique tauopathy – is caused by a similar
444 neuronal activity-related disease mechanism: plasma from an α-IgLON5 encephalitis patient
445 containing a polyclonal pool of α-IgLON5 AABs was able to trigger acute neuronal
446 hyperactivity. At high AAB doses or longer exposure, α-IgLON5 AABs led to neurotoxicity *in*
447 *vitro*. *In vivo*, these AABs induced neuroinflammation, motor deficits, and body weight loss.
448 Both neuronal silencing and inflammation were also affected on the gene expression level,
449 whereby animals that received α-IgLON5 AABs showed a distinct activation of complement 3,
450 MHC class II, and T cell receptor pathways. Similar responses of the innate immune system
451 were previously reported in transgenic mouse models of Tau pathology [24,36,37], indicating that
452 α-IgLON5 AABs induce an innate immune response that is typical for pro-pathological Tau
453 changes in the brain. Notably, this neuroinflammatory Tau signature occurred in parallel to p-
454 Tau accumulation, but not aggregation, in selected neuronal projections. Therefore, early Tau
455 changes – as observed in α-IgLON5 AAB treated animals - seem sufficient to induce a distinct
456 glia and immune cell response, which in turn may further accelerate Tau pathology and
457 neuronal damage.
458 Notably, the cerebroventricular infusion of AABs in the brain – as it was used in this study - is
459 currently limited to 2 weeks. Therefore, effects of long-term (or repeated) treatment with α-
460 IgLON5 AABs on Tau, neuroinflammation, and neurodegeneration are limited and new *in vivo*
461 models mirroring extended immune and activity stimulation in α-IgLON5 disease are required.
462

463 We identified α-IgLON5 AAB-induced neuronal hyperactivity as the driver of pro-pathological
464 Tau changes (somatodendritic p-Tau), a hallmark in α-IgLON5 disease. A similar
465 hyperactivity-induced Tau "activation", including Tau phosphorylation and resorting, may
466 occur in other AAB-induced neurological conditions as well – in this study we show similar

467 effects for α-LGI1 AABs-, suggesting a common route to Tau pathology in AEs. Indeed,
468 somatodendritic accumulation of p-Tau, accompanied by hippocampal atrophy, was found in
469 LGI1 patients [38]. It should be investigated whether Tau pathology in other immune-related
470 secondary tauopathies, e.g., subacute sclerosing panencephalitis (SSPE [39]; measles late
471 reaction) and head-nodding syndrome [40] (involving DJ-1 antibodies), occurs in response to
472 antibody-triggered neuronal hyperactivity as well.
473
474 Neuronal hyperactivity was previously suggested to also trigger Tau pathology in AD [41–43] and
475 in epilepsy [44]. The herein discovered route of action for α-IgLON5 AABs now adds another
476 example for activity-dependent Tau pathology, and, thereby, emphasizes the importance to
477 consider the modulation of neuronal activity for therapeutic approaches towards preventing or
478 lowering Tau pathology and toxicity in the brain. Next, it will be important to identify the
479 molecular mechanisms of how AAB binding to the surface protein IgLON5 can induce neuronal
480 activity, e.g., receptors and channels involved.
481
482 To which extent activity-induced Tau changes and excitotoxicity contribute to neurotoxicity in
483 α-IgLON5 disease and other AEs is unclear. Our data show that the effects of α-IgLON5 AABs
484 on neuronal function and Tau depends on AAB concentration and correlates with the amount
485 of hyperexcitation *in vitro*. Mice that received higher AAB doses showed stronger
486 neuroinflammation and motor symptoms. We propose that speed and extension of neuronal
487 dysfunction in AEs that are triggered by hyperexcitation-promoting AABs may depend on the
488 interplay between acute (minutes to hours) excitotoxicity and mid-term (days to weeks) Tau
489 toxicity, i.e., extreme, toxic hyperexcitation resulting in fast neuronal death versus moderate,
490 non-toxic hyperexcitation leading to Tau pathology and (slower) neuronal dysfunction.
491 Following this idea, hyperexcitation is apparently not immediately toxic in α-IgLON5 disease
492 and allows for the gradual development of pathological Tau changes. This would also mirror
493 the clinical observation that immunotherapy can be beneficial when initiated early in α-IgLON5
494 disease [5]. The extended presence of p-Tau in the somatodendritic compartment, however,
495 can exhaust the neuronal homeostasis network [45], induce synapse loss [46], or result in the
496 impairment of other key neuronal functions [47–49]. These Tau effects can ultimately induce
497 neurotoxicity also in α-IgLON5 disease.
498 In contrast, in α-LGI1 or α-GABA receptor AEs, extreme hyperexcitation may lead to
499 immediate neurotoxicity, so that a manifestation of later Tau pathology is less obvious or rare
500 in these diseases. For the treatment of patients with hyperexcitation-inducing AABs, like α-
501 IgLON5 and α-LGI1 AABs, determining the neuromodulatory activity of their AAB pool could

help in the choice of treatment, whether to target neuronal hyperexcitation, Tau phosphorylation and aggregation, or both.

Pathological Tau changes, including high phosphorylation, somatodendritic resorting, and later aggregation, occur in multiple neurological conditions. In neurodegenerative disease like AD and FTD, the location and extent of Tau pathology correlates with neuronal loss in the brain [8]. However, changes in Tau, although commonly classified as pathological, do not necessarily lead to immediate neuronal dysfunction and death [50,51]. They are, however, correlated with a progressive decay in synaptic homeostasis [46,52–54], ultimately leading to connectivity deficits and neuronal loss in AD and tauopathies. For α-IgLON5 AAB-induced Tau changes, a similar course of Tau action appears to apply. Long-term exposure to α-IgLON5 AABs (for weeks) was shown to result in neuronal p-Tau accumulation, disrupted synaptic protein homeostasis, decay in neuronal activity, and cell death, and caused cognitive deficits and anxiety-like behavior in mice [19,55,56]**.** These pathological changes can be interpreted as consequences of prolonged Tau activation, as they occur similarly in progressive neurodegenerative diseases like AD. Interestingly, we found that the activation of Tau (in form of somatodendritic re-sorting) lasted for multiple days even after removal of α-IgLON5 AABs, suggesting that activated Tau may play a role in a prolonged neuronal activity stress response. Whether a “deactivation” of Tau is facilitated by sorting it back to the axon or relies on Tau removal through degradation remains to be clarified. It also remains to be determined whether the persistence of the Tau response could be responsible for poor clinical response of the patient to the immunosuppression therapy, and whether Tau activation persists similarly in other AE disorders, e.g., LGI1 disease.

Our study shows that α-IgLON5 AABs activate Tau in selected hippocampal neural projections. p-Tau accumulation occurred in somata of DG granule cells and their MF projections onto CA3, which are important structures for learning and memory, and in commissural fibres in corpus callosum which are output structures of CA3. Similar hippocampal connections were recently suggested to be affected by α-IgLON5 AABs [55,56]. Additionally, we identified projections onto ventral CA1 (vCA1) and commissural fibres – probably coming from CA3 neurons [57,58] - as the main responders to α-IgLON5 AAB induced Tau phosphorylation. In mice, vCA1 neurons project to the entorhinal cortex, olfactory cortex, and amygdala, and are involved in anxiety, social, and motivational (e.g., feeding) behavior [57]. One may speculate that the accumulation of p-Tau in projections onto vCA1 could therefore correlate with anxiety-like behavior previously reported for mice treated with α-IgLON5 AABs [55], and could also be related to the rapid body weight loss we observed in such animals.

538 Notably, the hippocampal connections affected by α-IgLON5 AABs are similar to the ones
539 affected by Tau in AD, where Tau pathology starts in the entorhinal cortex and spreads
540 through the perforant pathway into DG granule cells and further through MFs into CA3 [59–61].
541 Furthermore, the anterior human hippocampus, which corresponds to the ventral
542 hippocampus in mice, shows metabolic changes and neuronal atrophy early in AD [62–64]. In
543 mice with α-IgLON5 AAB treatment, only projections onto CA1 of the ventral hippocampus
544 (vCA1) accumulated p-Tau. Considering that α-IgLON5 AABs activate Tau via neuronal
545 hyperactivity, this could be explained by the generally higher excitability of ventral compared
546 to dorsal CA1 hippocampal neurons [65]. Extending the link between neuronal hyperexcitation
547 and pro-pathological Tau activation, susceptibility of neurons to hyperexcitation could encode
548 the selective vulnerability of neuronal circuits to Tau pathology not just in α-IgLON5 disease
549 but also in AD and other tauopathies. In fact, hippocampal hyperactivity has been described
550 in patients with preclinical AD and mild cognitive impairment, stages of the disease where p-
551 Tau starts to accumulate in this region [66]. Similarly, recent MRI and PET imaging identified
552 that Aβ induces hyperactivity of the default mode network which propagates to the medial
553 temporal lobe and predicts Tau accumulation in early stages of AD [43,66].
554 Later in the disease progression, upon prolonged hippocampal Tau phosphorylation and
555 aggregation, synapse loss and a decline in neuronal activity can be observed. The herein
556 revealed mechanism, whereby α-IgLON5 AAB-induced neuronal hyperactivity is responsible
557 for pro-pathological Tau changes, therefore has important implications for the understanding
558 and treatment of Tau-related neurological conditions, far beyond α-IgLON5 disease. Future
559 work will need to identify how α-IgLON5 AAB binding induces neuronal hyperactivity on the
560 molecular level, whether these mechanisms are unique for α-IgLON5 AABs or can be applied
561 more general to different autoimmune antibodies, whether reversibility of the hyperexcitable
562 state can interrupt the Tau pathology cascade, and whether and when immunotherapy can
563 reverse progression of both autoimmunity and neurodegeneration.

564 Acknowledgement

565 We thank Britta Eickholt for providing us with access to instruments and equipment of the
566 Charité Biochemistry Department, the Advanced Medical Bioimaging Core Facility (AMBIO)
567 of the Charité, which enabled us to perform most microscopy on brain sections and neuron/cell
568 cultures, the Viral Core Facility (VCF) of the Charité for virus production, and the BIH
569 sequencing core for determining the RNA content of mouse brain tissue.
570

Funding

The work was funded by the German Center for Neurodegenerative diseases (DZNE) in the Helmholtz Society (to S.W. and H.P.), the Einstein Foundation Berlin (to B.A.), and the Deutsche Forschungsgemeinschaft (DFG; KFO 5023 BECAUSE-Y; Project 504745852 (to S.W. and H.P.). PR1274/5-1, PR1274/9-1, and PR1274/13-1 (to H.P.), the Helmholtz Association (HIL-A03 BaoBab to H.P.), and by the German Federal Ministry of Education and Research (Connect-Generate 01GM1908D, to H.P.). B.R.R. was supported by the Deutsche Forschungsgesellschaft (DFG; project 327654276 - SFB1315 and project 273915538 - SPP1926). H.-C.K. was supported by the German Research Council (DFG, FOR3004, KO2290/3-2).

Author contributions

Experiments/data. analysis of *in vitro* and *in vivo* α-IgLON5 AAB binding, Tau changes, neuroinflammation, RNAseq, Calcium imaging: Bilge Askin
Purification of IgLON5 AABs & Clinical experts: Alexander Goihl, Peter Körtvelyessy, Dirk Reinhold
Injection of mice and behavioral assessments: César Cordero Gómez
RNAseq analysis: Andrew Newman
Tissue processing, cryosectioning, immunohistochemistry (IHC) and IHC analysis: Cagla Kilic, Janne Lamberty, César Cordero Gómez, Sophie Lan-Linh Duong
NfL and GFAP ELISA: César Cordero Gómez
FACS for binding analysis: César Cordero Gómez
MFGE8 staining: Jessica Wagner, Jonas Neher
Epitope mapping and internalization experiments: Sophie Lan-Linh Duong
Establishing co-loc analysis pipelines and co-loc experiments: Valentine Thomas
Providing inputs for GCaMP experiments: Paul Turko
Autaptic neuron culture recordings: Benjamin R. Rost, Dietmar Schmitz
Supply of LGI1 AABs: Hans-Christian Kornau
Technical & neuron prep support: Sabrina Huebschmann, Ekaterina Semenova
General help, support, MS revision, discussion: Lisa Diez
Funding acquisition: Susanne Wegmann, Harald Prüss, Dietmar Schmitz, Benjamin R. Rost, Hans-Christian Kornau
Figure preparation: Bilge Askin, Susanne Wegmann, Cagla Kilic
Manuscript writing: Bilge Askin, Susanne Wegmann
Manuscript revision: all authors
Scientific concept: Susanne Wegmann, Harald Prüss, Bilge Askin, Peter Körtvelyessy,

References:

1. Prüss, H. Autoantibodies in neurological disease. *Nat Rev Immunol* **21**, 798–813 (2021).
2. Dalmau, J., Geis, C. & Graus, F. Autoantibodies to synaptic receptors and neuronal cell surface proteins in autoimmune diseases of the central nervous system. *Physiol Rev* **97**, 839–887 (2017).

612 3. Sabater, L. *et al.* A novel non-rapid-eye movement and rapid-eye-movement parasomnia
613 with sleep breathing disorder associated with antibodies to IgLON5: A case series,
614 characterisation of the antigen, and post-mortem study. *Lancet Neurol* **13**, 575–586
615 (2014).
616 4. Fu, Y., Zou, X. & Liu, L. Epileptic Seizures and Right-Sided Hippocampal Swelling as
617 Presenting Symptoms of Anti-IgLON5 Disease: A Case Report and Systematic Review of
618 the Literature. *Front Neurol* **13**, 1–9 (2022).
619 5. Grüter, T. *et al.* Clinical, serological and genetic predictors of response to immunotherapy
620 in anti-IgLON5 disease. *Brain* **146**, 600–611 (2023).
621 6. Madetko, N. *et al.* Anti-IgLON5 Disease – The Current State of Knowledge and Further
622 Perspectives. *Front Immunol* **13**, 1–8 (2022).
623 7. Gelpi, E. *et al.* Neuropathological criteria of anti-IgLON5-related tauopathy. *Acta*
624 *Neuropathol* **132**, 531–543 (2016).
625 8. Spillantini, M. G. & Goedert, M. Tau pathology and neurodegeneration. *Lancet Neurol* **12**,
626 609–622 (2013).
627 9. Iqbal, K. *et al.* Tau pathology in Alzheimer disease and other tauopathies. *Biochim Biophys*
628 *Acta Mol Basis Dis* **1739**, 198–210 (2005).
629 10. Zempel, H. Genetic and sporadic forms of tauopathies—TAU as a disease driver for the
630 majority of patients but the minority of tauopathies. *Cytoskeleton* 1–5 (2023)
631 doi:10.1002/cm.21793.
632 11. Vanaveski, T. *et al.* Promoter-Specific expression and genomic structure of Iglon family
633 genes in mouse. *Front Neurosci* **11**, 1–15 (2017).
634 12. Ranaivoson, F. M. *et al.* A Proteomic Screen of Neuronal Cell-Surface Molecules Reveals
635 IgLONs as Structurally Conserved Interaction Modules at the Synapse. *Structure* **27**, 893-
636 906.e9 (2019).
637 13. Venkannagari, H. *et al.* Highly Conserved Molecular Features in IgLONs Contrast Their
638 Distinct Structural and Biological Outcomes. *J Mol Biol* **432**, 5287–5303 (2020).
639 14. Landa, J. *et al.* Patients' IgLON5 autoantibodies interfere with IgLON5-protein interactions.
640 *Front Immunol* **14**, 1–7 (2023).
641 15. Hashimoto, T., Maekawa, S. & Miyata, S. IgLON cell adhesion molecules regulate
642 synaptogenesis in hippocampal neurons. *Cell Biochem Funct* **27**, 496–498 (2009).
643 16. Karis, K. *et al.* Altered expression profile of igLON family of neural cell adhesion molecules
644 in the dorsolateral prefrontal cortex of schizophrenic patients. *Front Mol Neurosci* **11**, 1–
645 12 (2018).
646 17. Sanz, R., Ferraro, G. B. & Fournier, A. E. IgLON Cell Adhesion Molecules Are Shed from
647 the Cell Surface of Cortical Neurons to Promote Neuronal Growth. *J Biol Chem* **290**, 4330
648 (2015).

649 18. Landa, J. *et al.* Effects of IgLON5 Antibodies on Neuronal Cytoskeleton: A Link between
650 Autoimmunity and Neurodegeneration. *Ann Neurol* **88**, 1023–1027 (2020).
651 19. Ryding, M. *et al.* Neurodegeneration Induced by Anti-IgLON5 Antibodies Studied in
652 Induced Pluripotent Stem Cell-Derived Human Neurons. *Cells* **10**, (2021).
653 20. Sabater, L., Planagumà, J., Dalmau, J. & Graus, F. Cellular investigations with human
654 antibodies associated with the anti-IgLON5 syndrome. *J Neuroinflammation* **13**, 1–12
655 (2016).
656 21. Wenke, N. K. *et al.* N-methyl-D-aspartate receptor dysfunction by unmutated human
657 antibodies against the NR1 subunit. *Ann Neurol* **85**, 771–776 (2019).
658 22. Wagner, J. *et al.* Medin co-aggregates with vascular amyloid-β in Alzheimer's disease.
659 *Nature* **612**, 123–131 (2022).
660 23. Brelstaff, J., Tolkovsky, A. M., Ghetti, B., Goedert, M. & Spillantini, M. G. Living Neurons
661 with Tau Filaments Aberrantly Expose Phosphatidylserine and Are Phagocytosed by
662 Microglia. *Cell Rep* **24**, 1939-1948.e4 (2018).
663 24. Chen, X. *et al.* Microglia-mediated T cell infiltration drives neurodegeneration in tauopathy.
664 *Nature 2023 615:7953* **615**, 668–677 (2023).
665 25. Zempel, H. & Mandelkow, E. Lost after translation: Missorting of Tau protein and
666 consequences for Alzheimer disease. *Trends in Neurosciences* vol. 37 721–732 Preprint
667 at https://doi.org/10.1016/j.tins.2014.08.004 (2014).
668 26. Gao, Y. *et al.* Targeted Reducing of Tauopathy Alleviates Epileptic Seizures and Spatial
669 Memory Impairment in an Optogenetically Inducible Mouse Model of Epilepsy. *Front Cell*
670 *Dev Biol* **8**, 1–10 (2021).
671 27. Zempel, H., Thies, E., Mandelkow, E. & Mandelkow, E. M. Aβ oligomers cause localized
672 Ca2+ elevation, missorting of endogenous Tau into dendrites, Tau phosphorylation, and
673 destruction of microtubules and spines. *Journal of Neuroscience* **30**, 11938–11950 (2010).
674 28. Kobayashi, S., Tanaka, T., Soeda, Y. & Takashima, A. Enhanced Tau Protein Translation
675 by Hyper-Excitation. *Front Aging Neurosci* **11**, (2019).
676 29. Hardingham, G. E., Arnold, F. J. L. & Bading, H. A calcium microdomain near NMDA
677 receptors: On switch for ERK-dependent synapse-to-nucleus communication. *Nat*
678 *Neurosci* **4**, 565–566 (2001).
679 30. Seagar, M. *et al.* LGI1 tunes intrinsic excitability by regulating the density of axonal Kv1
680 channels. *Proc Natl Acad Sci U S A* **114**, 7719–7724 (2017).
681 31. Fukata, Y. *et al.* Epilepsy-related ligand/receptor complex LGI1 and ADAM22 regulate
682 synaptic transmission. *Science* **313**, 1792–1795 (2006).
683 32. Schulte, U. *et al.* The epilepsy-linked Lgi1 protein assembles into presynaptic Kv1
684 channels and inhibits inactivation by Kvβ1. *Neuron* **49**, 697–706 (2006).

685 33. Kornau, H. C. *et al.* Human Cerebrospinal Fluid Monoclonal LGI1 Autoantibodies Increase
686 Neuronal Excitability. *Ann Neurol* **87**, 405–418 (2020).
687 34. Kreye, J. *et al.* Encephalitis patient-derived monoclonal GABAA receptor antibodies cause
688 epileptic seizures. *J Exp Med* **218**, (2021).
689 35. Ceanga, M. *et al.* Human NMDAR autoantibodies disrupt excitatory-inhibitory balance,
690 leading to hippocampal network hypersynchrony. *Cell Rep* **42**, (2023).
691 36. Wu, T. *et al.* Complement C3 Is Activated in Human AD Brain and Is Required for
692 Neurodegeneration in Mouse Models of Amyloidosis and Tauopathy. *Cell Rep* **28**, 2111-
693 2123.e6 (2019).
694 37. Dejanovic, B. *et al.* Complement C1q-dependent excitatory and inhibitory synapse
695 elimination by astrocytes and microglia in Alzheimer's disease mouse models. *Nature*
696 *Aging 2022 2:9* **2**, 837–850 (2022).
697 38. Day, G. S. *et al.* Flortaucipir (tau) PET in LGI1 antibody encephalitis. *Ann Clin Transl*
698 *Neurol* **8**, 491–497 (2021).
699 39. Bancher, C. *et al.* On the relationship between measles virus and Alzheimer neurofibrillary
700 tangles in subacute sclerosing panencephalitis. *Neurobiol Aging* **17**, 527–533 (1996).
701 40. Pollanen, M. S. *et al.* Nodding syndrome in Uganda is a tauopathy. *Acta Neuropathol* **136**,
702 691 (2018).
703 41. Styr, B. & Slutsky, I. Imbalance between firing homeostasis and synaptic plasticity drives
704 early-phase Alzheimer's disease. *Nat Neurosci* **21**, 463–473 (2018).
705 42. Lee, W. J. *et al.* Regional Aβ-tau interactions promote onset and acceleration of
706 Alzheimer's disease tau spreading. *Neuron* **110**, 1932-1943.e5 (2022).
707 43. Giorgio, J., Adams, J. N., Maass, A., Jagust, W. J. & Breakspear, M. Amyloid induced
708 hyperexcitability in default mode network drives medial temporal hyperactivity and early
709 tau accumulation. *Neuron* (2023) doi:10.1016/J.NEURON.2023.11.014.
710 44. Tai, X. Y. *et al.* Hyperphosphorylated tau in patients with refractory epilepsy correlates with
711 cognitive decline: a study of temporal lobe resections. *Brain* **139**, 2441–2455 (2016).
712 45. Papanikolopoulou, K. & Skoulakis, E. M. C. Altered Proteostasis in Neurodegenerative
713 Tauopathies. *Adv Exp Med Biol* **1233**, 177–194 (2020).
714 46. Yoshiyama, Y. *et al.* Synapse Loss and Microglial Activation Precede Tangles in a P301S
715 Tauopathy Mouse Model. *Neuron* **53**, 337–351 (2007).
716 47. Meier, S. *et al.* Pathological tau promotes neuronal damage by impairing ribosomal
717 function and decreasing protein synthesis. *Journal of Neuroscience* **36**, 957–962 (2016).
718 48. Vanderweyde, T. *et al.* Interaction of tau with the RNA-Binding Protein TIA1 Regulates tau
719 Pathophysiology and Toxicity. *Cell Rep* **15**, 1455–1466 (2016).
720 49. Eftekharzadeh, B. *et al.* Tau Protein Disrupts Nucleocytoplasmic Transport in Alzheimer's
721 Disease. *Neuron* **99**, 925-940.e7 (2018).

722 50. Kuchibhotla, K. V. *et al.* Neurofibrillary tangle-bearing neurons are functionally integrated
723 in cortical circuits in vivo. *Proc Natl Acad Sci U S A* **111**, 510–514 (2014).
724 51. Arendt, T. *et al.* Reversible paired helical filament-like phosphorylation of tau is an adaptive
725 process associated with neuronal plasticity in hibernating animals. *Journal of*
726 *Neuroscience* **23**, 6972–6981 (2003).
727 52. Henstridge, C. M., Pickett, E. & Spires-Jones, T. L. Synaptic pathology: A shared
728 mechanism in neurological disease. *Ageing Res Rev* **28**, 72–84 (2016).
729 53. Pickett, E. K. *et al.* Spread of tau down neural circuits precedes synapse and neuronal
730 loss in the rTgTauEC mouse model of early Alzheimer's disease. *Synapse* **71**, (2017).
731 54. Dejanovic, B. *et al.* Changes in the Synaptic Proteome in Tauopathy and Rescue of Tau-
732 Induced Synapse Loss by C1q Antibodies. *Neuron* **100**, 1322-1336.e7 (2018).
733 55. Ni, Y. *et al.* Anti-IgLON5 antibodies cause progressive behavioral and neuropathological
734 changes in mice. *J Neuroinflammation* **19**, 1–18 (2022).
735 56. Alvente, S. *et al.* Pilot Study of the Effects of Chronic Intracerebroventricular Infusion of
736 Human Anti-IgLON5 Disease Antibodies in Mice. *Cells* **11**, (2022).
737 57. Masurkar, A. V. Towards a circuit-level understanding of hippocampal CA1 dysfunction in
738 Alzheimer's disease across anatomical axes. *J Alzheimers Dis Parkinsonism* **8**, 412–412
739 (2018).
740 58. Dong, H. W., Swanson, L. W., Chen, L., Fanselow, M. S. & Toga, A. W. Genomic-anatomic
741 evidence for distinct functional domains in hippocampal field CA1. *Proc Natl Acad Sci U S*
742 *A* **106**, 11794–11799 (2009).
743 59. Hyman, B. T., Kromer, L. J. & Van Hoesen, G. W. A direct demonstration of the perforant
744 pathway terminal zone in Alzheimer's disease using the monoclonal antibody Alz-50. *Brain*
745 *Res* **450**, 392–397 (1988).
746 60. Thal, D. R. *et al.* Alzheimer-related tau-pathology in the perforant path target zone and in
747 the hippocampal stratum oriens and radiatum correlates with onset and degree of
748 dementia. *Exp Neurol* **163**, 98–110 (2000).
749 61. De Calignon, A. *et al.* Propagation of Tau Pathology in a Model of Early Alzheimer's
750 Disease. *Neuron* **73**, 685–697 (2012).
751 62. Ouchi, Y. *et al.* Altered glucose metabolism in the hippocampal head in memory
752 impairment. *Neurology* **51**, 136–142 (1998).
753 63. Wang, L. *et al.* Changes in hippocampal volume and shape across time distinguish
754 dementia of the Alzheimer type from healthy aging. *Neuroimage* **20**, 667–682 (2003).
755 64. Greene, S. J., Killiany, R. J., Alzheimer, T., Disease Neuroimaging Initiative, S. & Lilly, E.
756 Hippocampal Subregions are Differentially Affected in the Progression to Alzheimer's
757 Disease. *The Anatomical Record: Advances in Integrative Anatomy and Evolutionary*
758 *Biology* **295**, 132–140 (2012).

759 65. Dougherty, K. A., Islam, T. & Johnston, D. Intrinsic excitability of CA1 pyramidal neurones
760 from the rat dorsal and ventral hippocampus. *J Physiol* **590**, 5707–5722 (2012).
761 66. Targa Dias Anastacio, H., Matosin, N. & Ooi, L. Neuronal hyperexcitability in Alzheimer's
762 disease: what are the drivers behind this aberrant phenotype? *Translational Psychiatry*
763 *2022 12:1* **12**, 1–14 (2022).
764 67. Ly, L. T. *et al.* Affinities of human NMDA receptor autoantibodies: implications for disease
765 mechanisms and clinical diagnostics. *J Neurol* **265**, 2625–2632 (2018).
766 68. Jin, Y., Tam, O. H., Paniagua, E. & Hammell, M. TEtranscripts: a package for including
767 transposable elements in differential expression analysis of RNA-seq datasets.
768 *Bioinformatics* **31**, 3593–3599 (2015).
769 69. Patel, T. P., Man, K., Firestein, B. L. & Meaney, D. F. Automated quantification of neuronal
770 networks and single-cell calcium dynamics using calcium imaging. *J Neurosci Methods*
771 **243**, 26–38 (2015).
772 70. Rost, B. R. *et al.* Autaptic cultures of single hippocampal granule cells of mice and rats.
773 *European Journal of Neuroscience* **32**, 939–947 (2010).
774

Figures

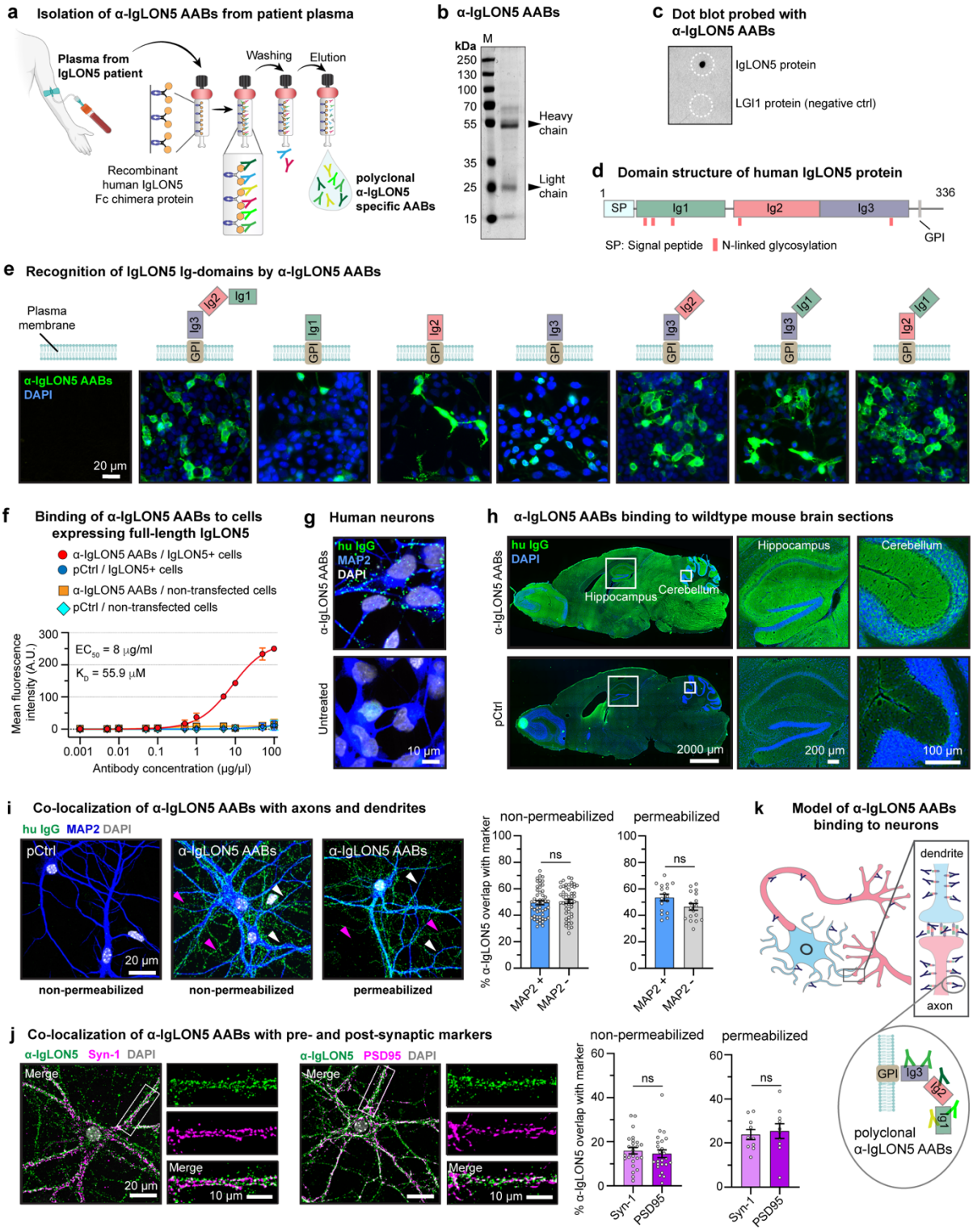

Figure 1. Purification and verification of α-IgLON5 AABs from patient plasma. a, Principle of α-IgLON5 AAB isolation from clinically verified IgLON5 patient plasma using affinity purification on immobilized recombinant human IgLON5 Fc-chimera proteins. **b,** SDS-PAGE of isolated antibodies. **c,** Dot blot of recombinant IgLON5 and LGI protein (negative control) shows specific reactivity of the

782 isolated α-IgLON5 AABs against IgLON5. **d,** Illustration of human IgLON5 protein (336 amino acids)
783 consisting of a signal peptide for secretion (SP), three extracellular Ig domains (Ig1/2/3), and a GPI-
784 anchor (GPI) in the C-terminus, tethering IgLON5 to the plasma membrane. **e,** Binding of α-IgLON5
785 AABs in HEK293T cells overexpressing full-length IgLON5 protein or (combinations of) individual Ig
786 domains. Scale bar = 20 μm. **f,** FACS binding affinity characterization (EC_{50} = 8 μg/ml; K_D=55.9 μM) of
787 α-IgLON5 AABs to HEK cells expressing full-length human IgLON5 (IgLON5+). Control patient IgGs
788 (pCtrl) did not show binding. Data shown as mean±SEM, N=3 independent experiments. **g,** α-IgLON5
789 AABs recognize endogenous IgLON5 in human neuronal stem cells (hNSCs). **h,** Immunoreactivity of
790 α-IgLON5 AABs compared to pCtrl in fresh frozen sagittal brain sections from an adult wildtype mouse.
791 **i,** Primary hippocampal mouse neurons (DIV12-15) treated with α-IgLON5 AABs show similar α-IgLON5
792 AABs binding to dendritic (MAP2+; white arrow heads) and axonal regions (MAP2-; pink arrow heads).
793 Data were obtained from three independent experiments shown as mean±SEM. Student's T-test. **j,**
794 Immunofluorescence shows similar partial co-localization of α-IgLON5 AAB with pre-synaptic
795 (Synapsin-1) and post-synaptic (PSD-95) markers, both in (i) non-permeabilized (~15%) and (ii)
796 permeabilized (~22%) primary mouse neurons. Data shown as mean±SEM, N=3 independent
797 experiments, Student T-test. **k,** Model: Polyclonal α-IgLON5 AABs from patient serum bind to different
798 Ig domains of IgLON5 on the neuronal surface.
799
800
801
802
803
804
805
806
807
808
809
810
811
812

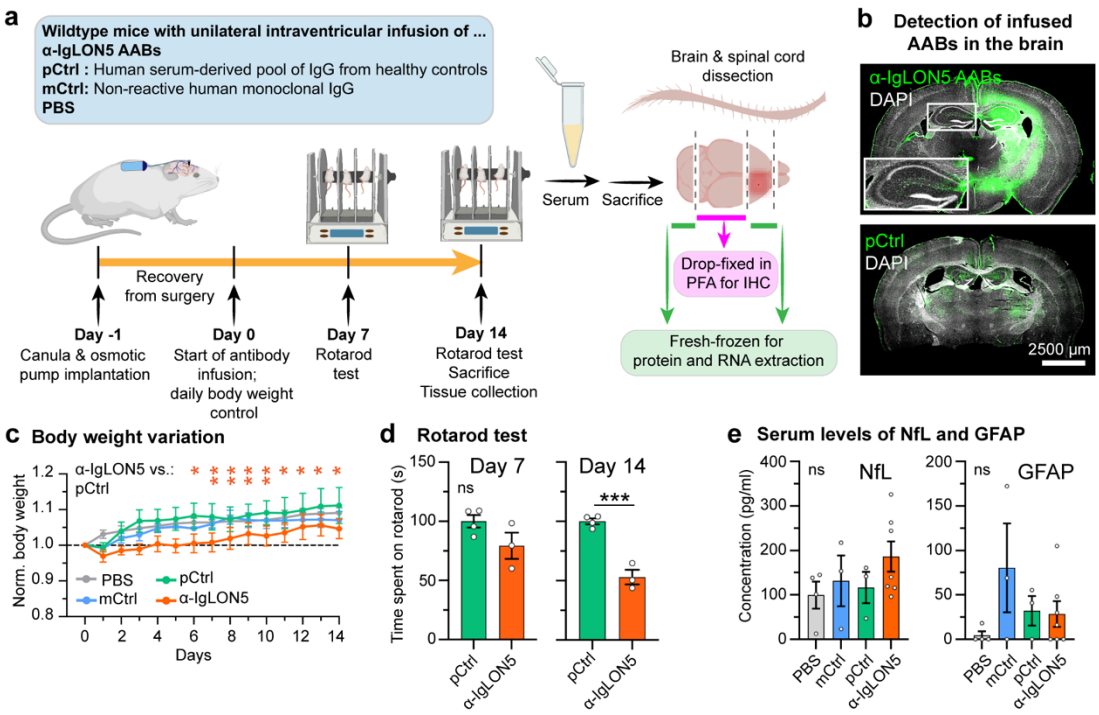

Figure 2. Intraventricular infusion of α-IgLON5 and control AABs into wildtype mice. a, Experimental design for the *in vivo* application of α-IgLON5 AABs. Wildtype mice were infused in the right ventricle with α-IgLON5 AABs, control antibodies (pCtrl, mCtrl), or PBS. 75 µg AABs were infused for 14 consecutive days with a flow rate of 0.25 µl/h. Body weight was monitored daily starting on Day 0. At Day 7 and Day 14, rotarod experiments were conducted and serum samples were collected before animals were sacrificed. Brain and spinal cord tissues were dissected for later investigation by immunofluorescence, and for protein and RNA analysis. **b,** Immunofluorescence images of coronal mouse brain sections show the distribution of infused α-IgLON5 AAB and pCtrl in the brain after 14 days (fluorescence anti-human IgG secondary antibody). Inset shows labeling of cells in the contralateral hippocampus in α-IgLON5 AAB infused brain. **c,** Body weight relative to Day 0 measured during 14 days of treatment. Data shown as mean±SEM, N=3-6 animals per group, Multiple t-test comparing IgLON5 and pCtrl at each time point. **d,** Rotarod performance (time spent on rod) of α-IgLON5 AAB and pCtrl animals determined at Day 7 and Day 14. Data shown as mean±SEM, N=3-4 animals per group. Student T-test. **e,** Serum levels of NfL and GFAP determined by ELISA. Data shown as mean±SEM, N=3-6 animals, with 3 technical replicates measured per animal.

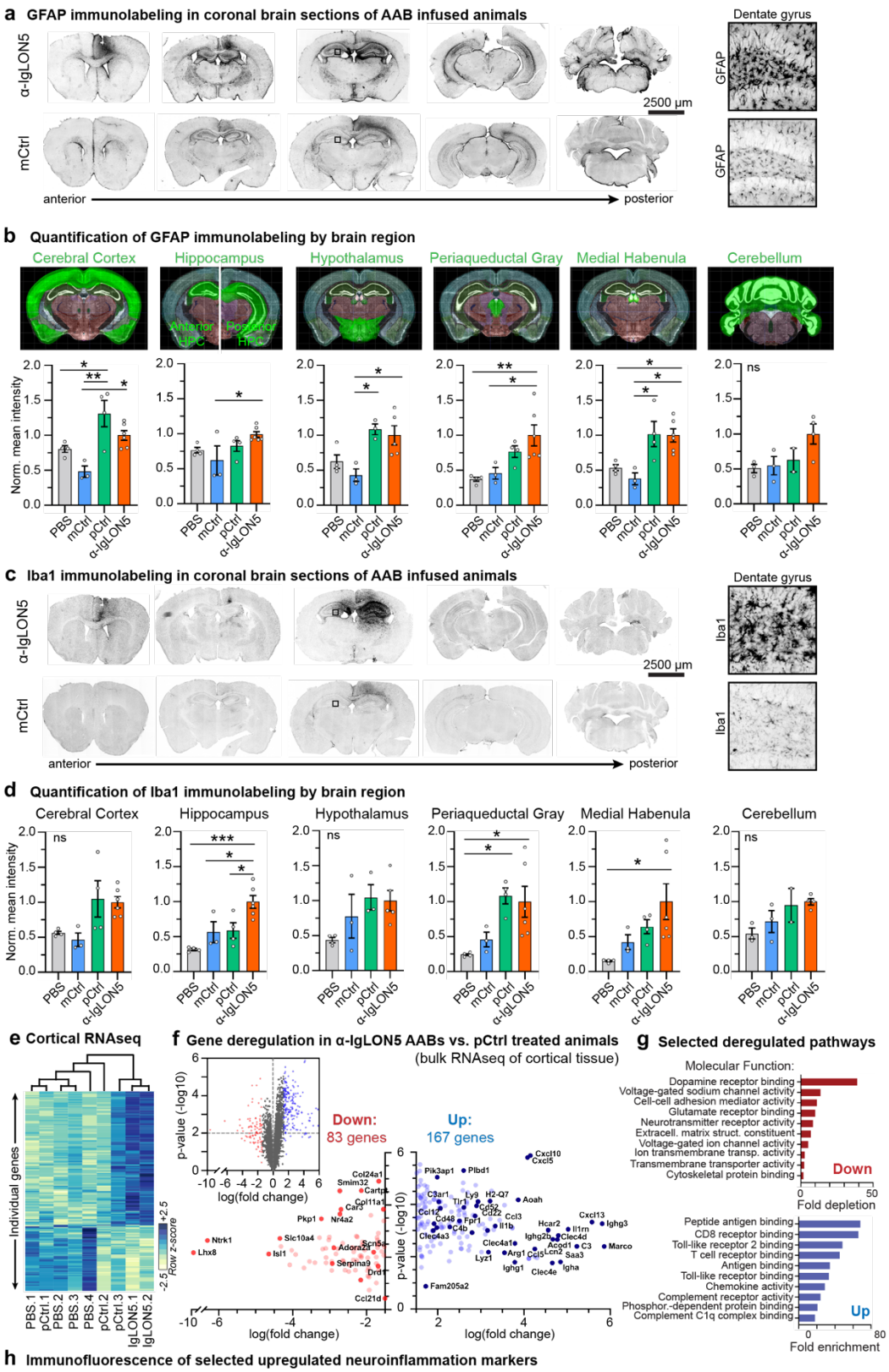
a GFAP immunolabeling in coronal brain sections of AAB infused animals
α-IgLON5
mCtrl
anterior
posterior
2500 µm
Dentate gyrus
GFAP
b Quantification of GFAP immunolabeling by brain region
Cerebral Cortex
Hippocampus
Hypothalamus
Periaqueductal Gray
Medial Habenula
Cerebellum
Norm. mean intensity
PBS
mCtrl
pCtrl
α-IgLON5
ns
c Iba1 immunolabeling in coronal brain sections of AAB infused animals
Iba1
d Quantification of Iba1 immunolabeling by brain region
e Cortical RNAseq
Individual genes
Row z-score
f Gene deregulation in α-IgLON5 AABs vs. pCtrl treated animals
(bulk RNAseq of cortical tissue)
Down:
83 genes
Up:
167 genes
p-value (-log10)
log(fold change)
g Selected deregulated pathways
Molecular Function:
Dopamine receptor binding
Voltage-gated sodium channel activity
Cell-cell adhesion mediator activity
Glutamate receptor binding
Neurotransmitter receptor activity
Extracell. matrix struct. constituent
Voltage-gated ion channel activity
Ion transmembrane transp. activity
Transmembrane transporter activity
Cytoskeletal protein binding
Down
Fold depletion
Peptide antigen binding
CD8 receptor binding
Toll-like receptor 2 binding
T cell receptor binding
Antigen binding
Toll-like receptor binding
Chemokine activity
Complement receptor activity
Phosphor.-dependent protein binding
Complement C1q complex binding
Up
Fold enrichment
h Immunofluorescence of selected upregulated neuroinflammation markers
DG
CA1
C3
Iba1
DAPI
CD68
C1q
CD8
200 µm
5 µm
50 µm
Rel. C1q intensity

830

831 **Figure 3. Neuroinflammatory changes in brain upon α-IgLON5 AAB infusion. a,** Representative
832 brain sections immunolabeled for GFAP (astrocytes). **b,** Quantification of GFAP intensity in different
833 regions of α-IgLON5 AAB and control brains. Data shown as mean±SEM, N=3-6 animals, 3-5 brain
834 sections per animal. One-way ANOVA with Tukey post-test. Location of brain regions is shown in
835 images below graphs (adapted from 3D-brain Explorer, Allen Mouse Brain Atlas). **c,** Representative
836 brain sections immunolabeled for Iba1 (microglia). **d,** Quantification of Iba1 intensity in different regions
837 of α-IgLON5 AAB and control brains. Data shown as mean±SEM, N=3-6 animals, 3-5 brain sections
838 per animal. One-way ANOVA with Tukey post-test. **e,** Heat map showing differential gene expression
839 in contralateral cortical tissue in individual animals from α-IgLON5, pCtrl and PBS groups **f,** Volcano
840 plots of differentially expressed genes in the cortex of α-IgLON5 AAB infused animals. **g,** Gene ontology
841 (GO) enrichment analysis of the differentially expressed genes showing deregulated pathways in α-
842 IgLON5 AAB infused animals. **h**, Immunolabeling of neuroinflammatory markers (C3, C1q, CD68 and
843 CD8) upregulated in α-IgLON5 vs. mCtrl AAB treated animals. White arrow heads indicate C3-positive
844 astrocytes (left panel) and CD8-positive T cells (right panel). For quantification of C1q fluorescence,
845 data shown as mean±SD, N=3-5 hippocampal brain sections per group. One-way ANOVA with Tukey
846 post-test. Scale bars as indicated.
847

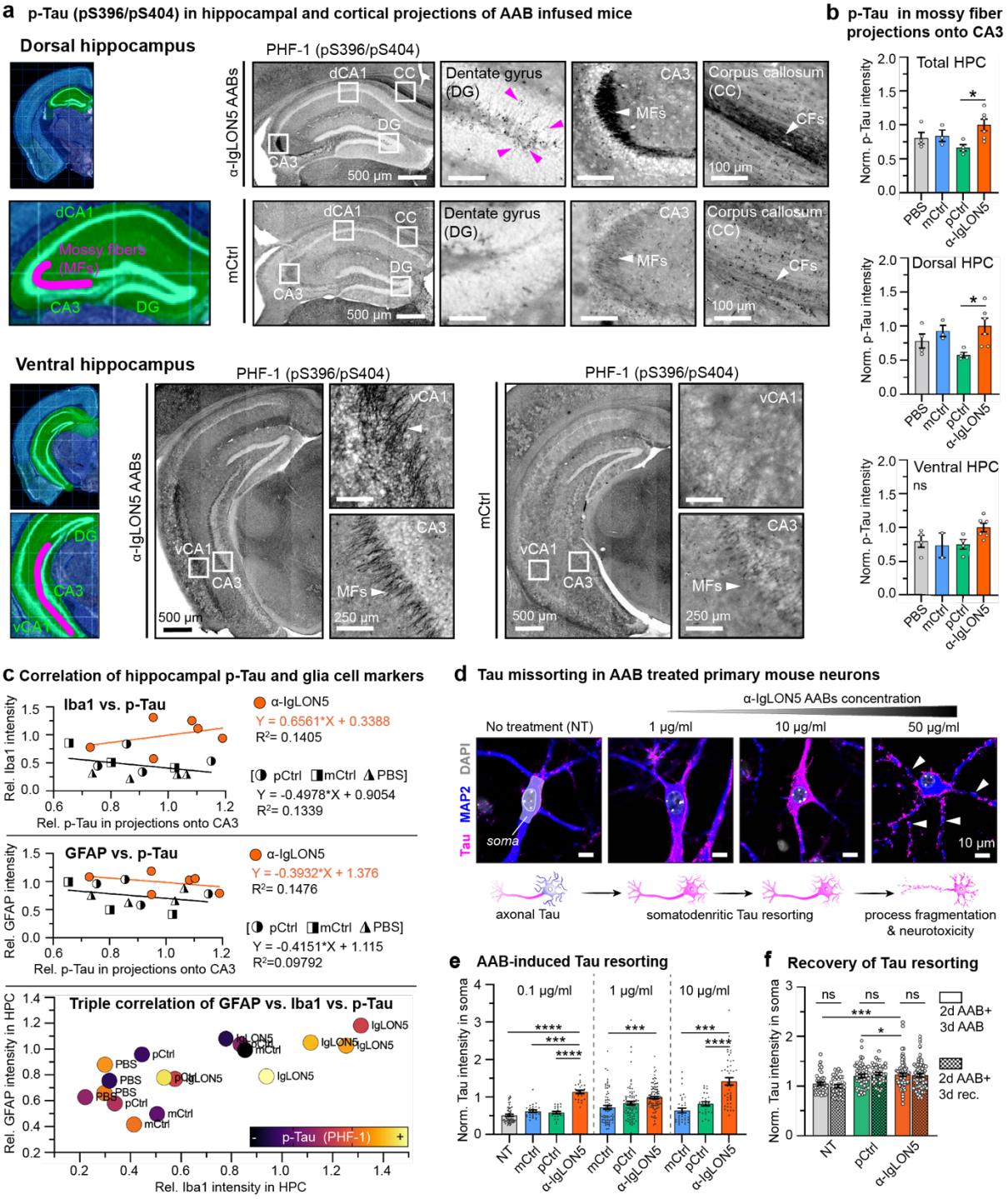

Figure 4. α-IgLON5 AABs induce phosphorylation and somatodendritic resorting of Tau in hippocampal neurons. a, Representative images of p-Tau pS396/pS404 (PHF-1) immunoreactivity in α-IgLON5 AAB and control brains. Top: p-Tau accumulation in dorsal hippocampus in dentate gyrus (DG) granule cells (left; white arrow heads), mossy fiber (MF) projections onto CA3 (center; white arrowhead), and in commissural fiber (CF) tracks of the corpus callosum (CC; right, white arrowhead). No p-Tau is found in dorsal CA1 (dCA1). Bottom: p-Tau accumulation in ventral hippocampus in projections onto ventral CA1 (vCA1; white arrow head) and MF projections onto CA3 (white arrow head). Scale bars as indicated. **b,** Quantification of mean p-Tau pS396/pS404 (PHF-1) intensity in

858 projections onto CA3. Data presented as mean±SEM, N=3-6 animals. One-way ANOVA with Tukey
859 post-test. **c,** Correlation between hippocampal Iba1 (top) or GFAP (middle) intensities and p-Tau
860 pS396/pS404 in projections onto CA3 for α-IgLON5 animals (orange data points and linear fit) vs.
861 combined control groups (black-white data points and black line fit). Bottom: triple correlation with p-
862 Tau levels color-coded. Note that IgLON5 animals cluster in the top right of the graph with red/yellow
863 color coding, indicating elevated hippocampal GFAP and Iba1 levels and above-average p-Tau levels
864 in projection onto CA3 in animals that received α-IgLON5 AABs. Linear fit values are indicated. **d,**
865 Representative images of primary hippocampal neurons treated with different concentrations (1, 10,
866 and 50 μg/μl) of α-IgLON5 AABs and immunolabeled for MAP2 (blue), Tau (magenta), and DNA (DAPI,
867 white). White solid line and shaded ROI in non-treated neurons (NT) indicate ROIs manually defined
868 for measuring the intensity of Tau in the soma. At 50 μg/μl**,** fragmentation of neuronal processes (white
869 arrow heads) indicated neurotoxicity. **e,** Quantification of Tau re-sorting into the soma in primary
870 neurons after treatment with 0.1, 1, or 10 μg/ml α-IgLON5 AABs and controls for 2 days. N=3
871 independent experiments, data presented as mean±SEM, One-way ANOVA with Tukey post-test **f,**
872 Quantification of Tau re-sorting into the soma in primary neurons after treatment with 1 μg/ml α-IgLON5
873 AAB and control antibodies for 5 days (bars without pattern fill) or after 2 days antibody treatment and
874 3 days recovery (bars with pattern fill). Data collected from 2 independent experiments and presented
875 as mean±SEM. One-way ANOVA with Tukey post-test.
876

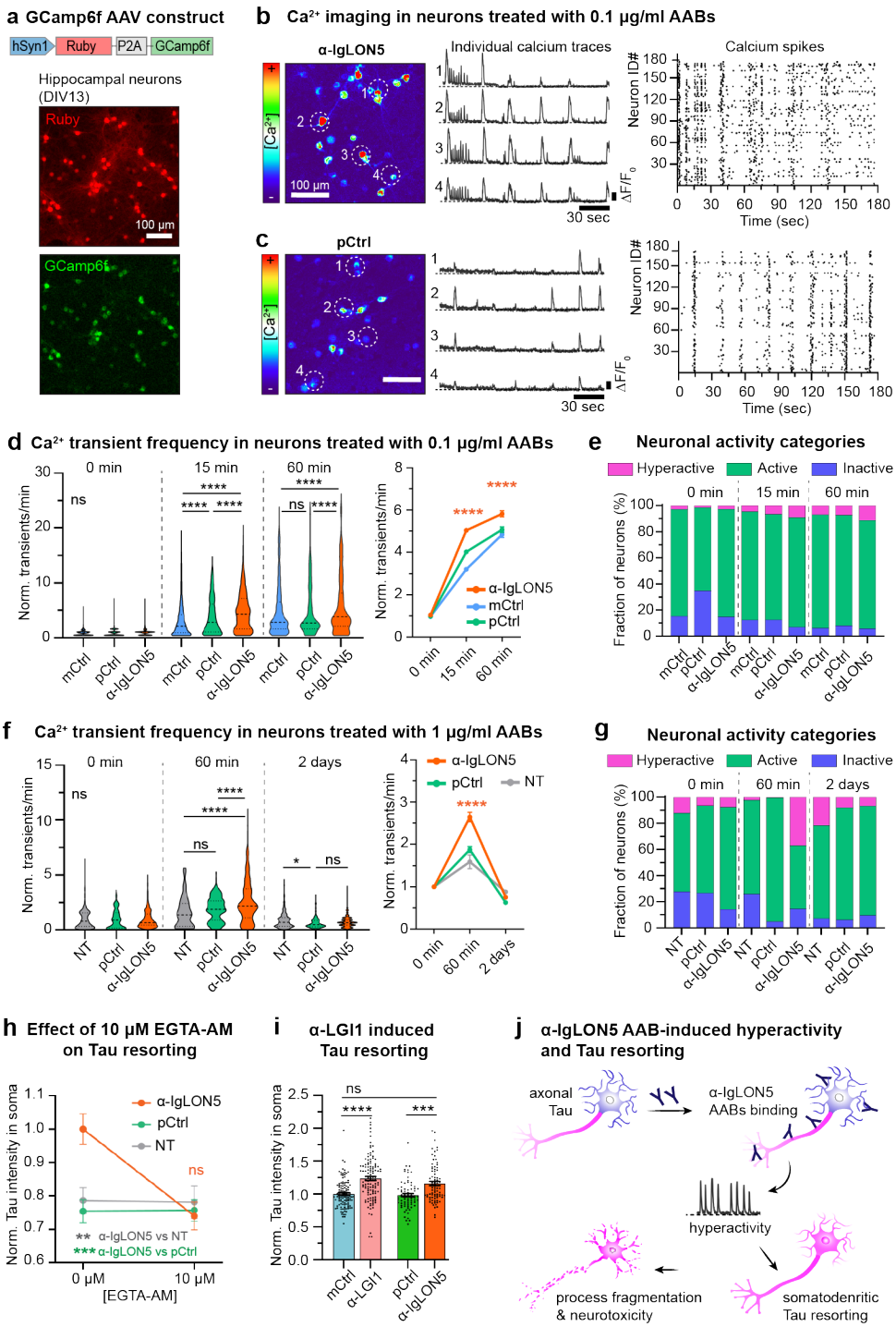

Figure 5. α-IgLON5 AAB-induced neuronal hyperactivity. a, Construct design for genetically encoded Ca^{2+} indicator (GCamp6f). **b** Representative z-projection (sum) of Ca^{2+} recordings, individual activity traces and raster plots for detected calcium spikes after 15 min 0.1 µg/ml α-IgLON5 and **c,** pCtrl treatment. **d,** Frequency (transients/min) of spontaneous Ca^{2+} transients in neurons before (0 min) and after 0.1 µg/ml AAB treatment for 15 min and 60 min. NT = untreated neurons Violin plot (left) shows data distribution in treatment groups. Line plot (right) shows mean±SEM for each group and time point. N=3 independent experiments with 1094 to 1379 neurons per condition and time point. One-way ANOVA with Tukey post-test. **e,** Percentage (%) of inactive (blue), active (green), and hyperactive (pink)

887 neurons in cultures treated with 0.1 μg/ml α-IgLON5 AABs or controls for 0, 15, or 60 min**.** Hyperactive
888 criteria: Number of transients/min > mean+2*SD of pCtrl at each recording time point. Active: 0 <
889 number of transients/min < mean+2*SD of pCtrl at each recording time point. Silent: no transients. **f,**
890 Frequency (transients/min) of spontaneous Ca^{2+} transients in neurons before (0 min) and after 1 μg/ml
891 α-IgLON5 AAB treatment for 60 min or 2 days. N=3 independent experiments with 71 to 994 neurons
892 per condition and time point. One-way ANOVA with Tukey post-test. **g,** Percentage (%) of inactive
893 (blue), active (green), and hyperactive (pink) neurons in cultures treated with 1 μg/ml antibody or
894 controls for 0 or 60 min or 2 days**. h,** Quantification of Tau re-sorting into the soma in neurons treated
895 with 1 μg/ml α-IgLON5 after suppressing their activity with 10 μM EGTA-AM pre-treatment for 20 min.
896 Data collected from two independent experiments with 47 to 60 neurons per condition and presented
897 as mean±SEM. One-way ANOVA with Tukey post-test **i,** Quantification of Tau re-sorting after treatment
898 with monoclonal 1 μg/ml α-LGI1 AAB, α-IgLON5 AAAB, and controls (mCtrl and pCtrl) for 2 days. Data
899 collected from two independent experiments and presented as mean±SEM, One-way ANOVA with
900 Tukey post-test. **j,** Model: Binding of α-IgLON5 AABs triggers acute neuronal hyperactivity (in minutes),
901 which induces prolonged Tau phosphorylation and somatodendritic resorting (=Tau activation) for days.
902 Excessive or repeated α-IgLON5 AABs exposure leads to acute excitotoxicity and/or permanent Tau
903 activation resulting in neuronal death.
904
905
906

Supplementary Figures

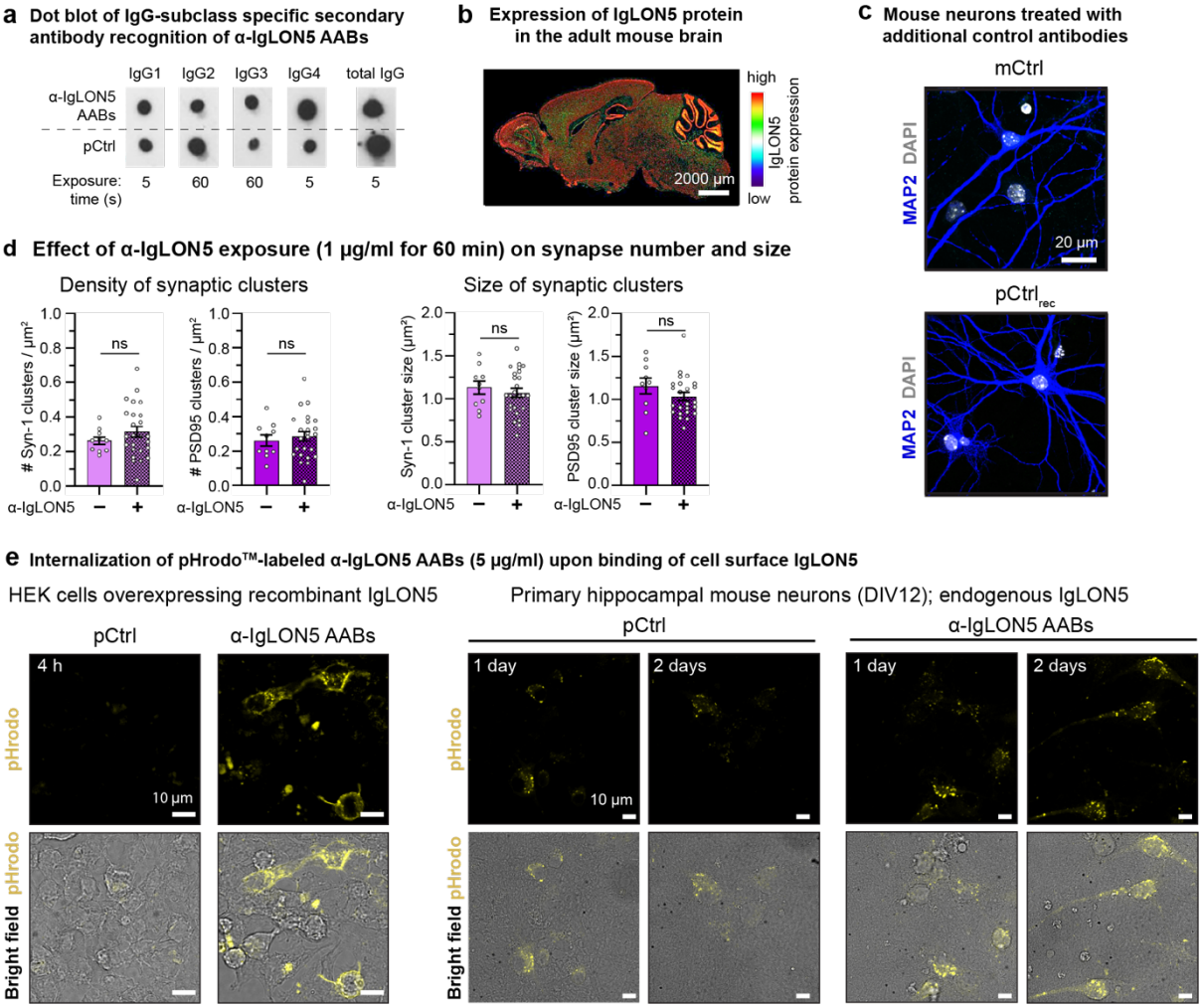

Supplementary Figure S1. α-IgLON5 AABs IgG subclass analysis and expression in adult mouse brain. a, Dot blot of patient-derived α-IgLON5 AABs and a control IgG pool isolated from serum of healthy control individuals (pCtrl) detected with IgG subclass-specific secondary antibodies. **b,** Spatial distribution of IgLON5 protein expression in the adult mouse brain (Allen mouse brain atlas: http://mouse.brain-map.org/experiment/show?id=71380538). Scale bar = 2000 µm. **c,** Additional control antibodies tested did not bind to cultured hippocampal mouse neurons: monoclonal human non-reactive AAB (mCtrl) [21] and commercially available normal human IgG ($pCtrl_{rec}$). Scale bars = 20 µm. **d,** Pre- (Synapsin-1) and post-synaptic (PSD95) cluster numbers and sizes did not change upon acute α-IgLON5 AAB exposure (1 µg/ml for 60 min). Data collected from three independent experiments and shown as mean±SEM, Student T-test. **e,** Representative images showing internalization and lysosomal acidification (=fluorescence) of pHrodo™-labelled α-IgLON5 or pCtrl in HEK293 cells overexpressing full-length IgLON5 after 4 h (left) and in primary hippocampal mouse neurons after 1 day and 2 days (right). Scale bars = 10 µm.

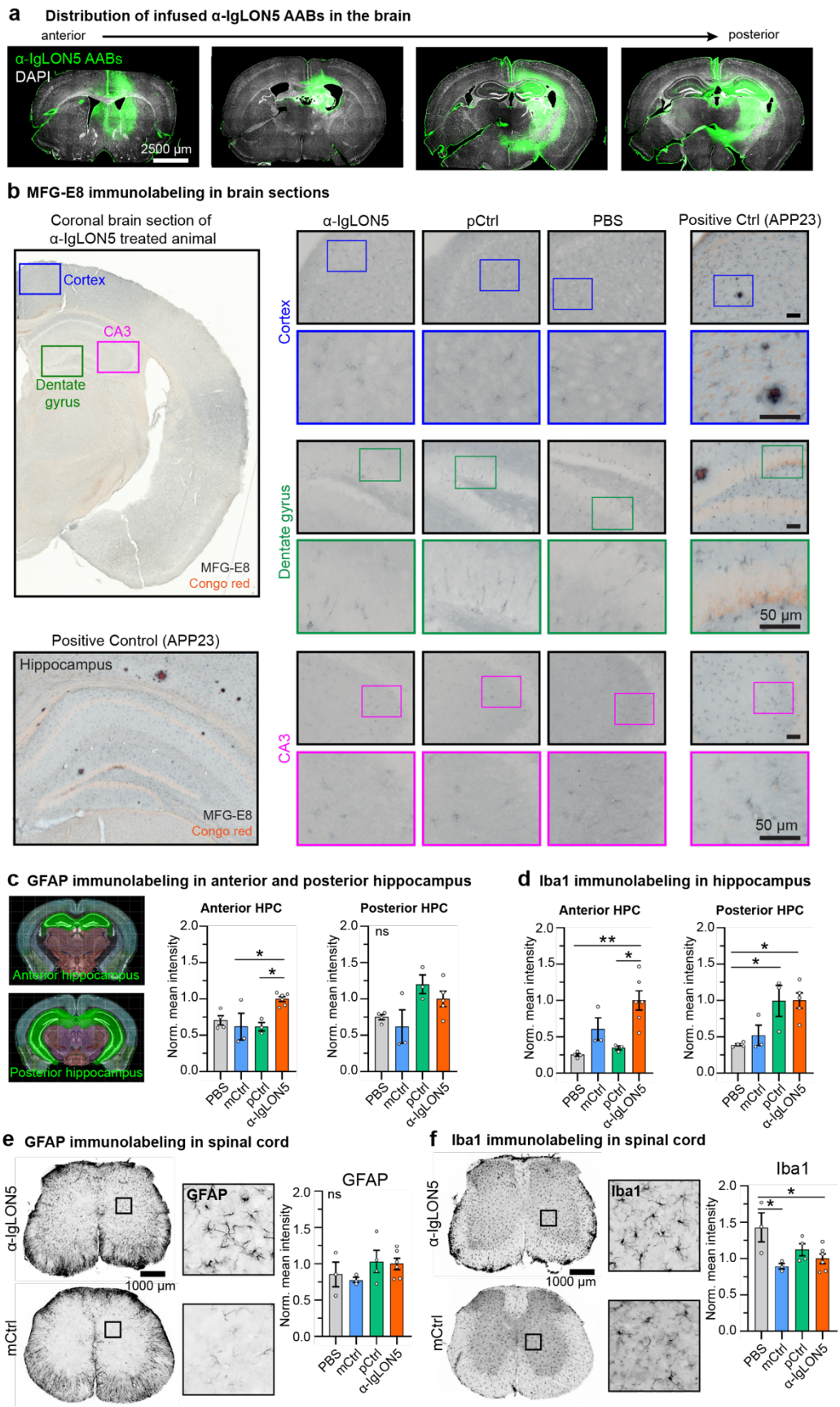
a Distribution of infused α-IgLON5 AABs in the brain
anterior
posterior
α-IgLON5 AABs
DAPI
2500 µm
b MFG-E8 immunolabeling in brain sections
Coronal brain section of α-IgLON5 treated animal
Cortex
CA3
Dentate gyrus
MFG-E8
Congo red
α-IgLON5
pCtrl
PBS
Positive Ctrl (APP23)
Cortex
Dentate gyrus
CA3
50 µm
Positive Control (APP23)
Hippocampus
c GFAP immunolabeling in anterior and posterior hippocampus
Anterior hippocampus
Posterior hippocampus
Anterior HPC
Posterior HPC
Norm. mean intensity
ns
PBS
mCtrl
pCtrl
α-IgLON5
d Iba1 immunolabeling in hippocampus
e GFAP immunolabeling in spinal cord
GFAP
1000 µm
f Iba1 immunolabeling in spinal cord
Iba1

927 **Supplemental Figure S2. MFEG-8 immunolabeling in brain sections of AAB treated mice. a,**
928 Images of coronal mouse brain sections (from anterior to posterior) show distribution of infused α-
929 IgLON5 AABs in the brain after 14 days (fluorescence anti-human IgG secondary antibody). **b,** Location
930 of anterior and posterior hippocampal regions shown in images on the left (adapted from 3D-brain
931 Explorer, Allen Mouse Brain Atlas). Quantification of GFAP (astrocytes) and **c,** Iba1 (microglia) intensity
932 in anterior and posterior hippocampus of α-IgLON5 AAB and control brains. Data shown as mean±SEM,
933 N=3-6 animals, 2-3 brain sections per animal. One-way ANOVA with Tukey post-test. **d,**
934 Immunolabelling of MFGE-8 and co-staining with congo red in α-IgLON5 AAB and control brains, in
935 cortex, dentate gyrus and CA3 (Schaffer collaterals). APP23 mouse brain section was used as a
936 positive control **e**, Representative images, and quantification of GFAP and **f,** Iba1 immunolabeling in
937 spinal cord sections of α-IgLON5 AAB and control animals. Data shown as mean±SEM, N=3-4 animals,
938 5-8 spinal cord sections per animal. One-way ANOVA with Tukey post-test.

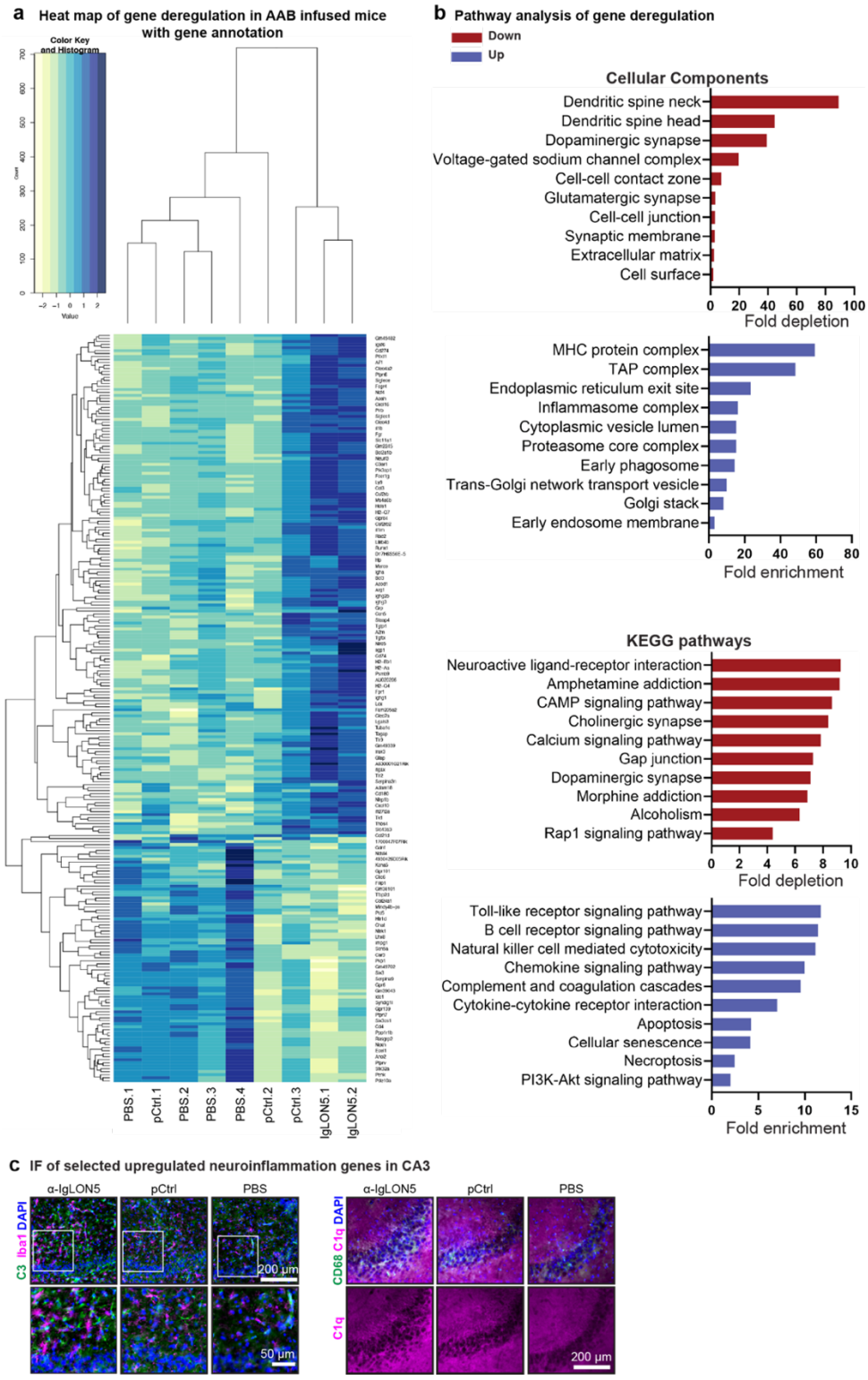

Supplementary Figure S3. **Gene and pathway deregulation detected by bulk RNAseq of cortical tissue. a,** Heat map showing differential gene expression in contralateral cortical tissue in individual animals from α-IgLON5, pCtrl, and PBS groups. **b,** Gene ontology (GO) enrichment analysis for cellular components and KEGG pathways in α-IgLON5 AAB infused animals. **c**, Immunolabeling of inflammatory markers (C3, C1q, CD68) in hippocampal CA3 region, upregulated in α-IgLON5 vs. pCtrl AAB treated mice.

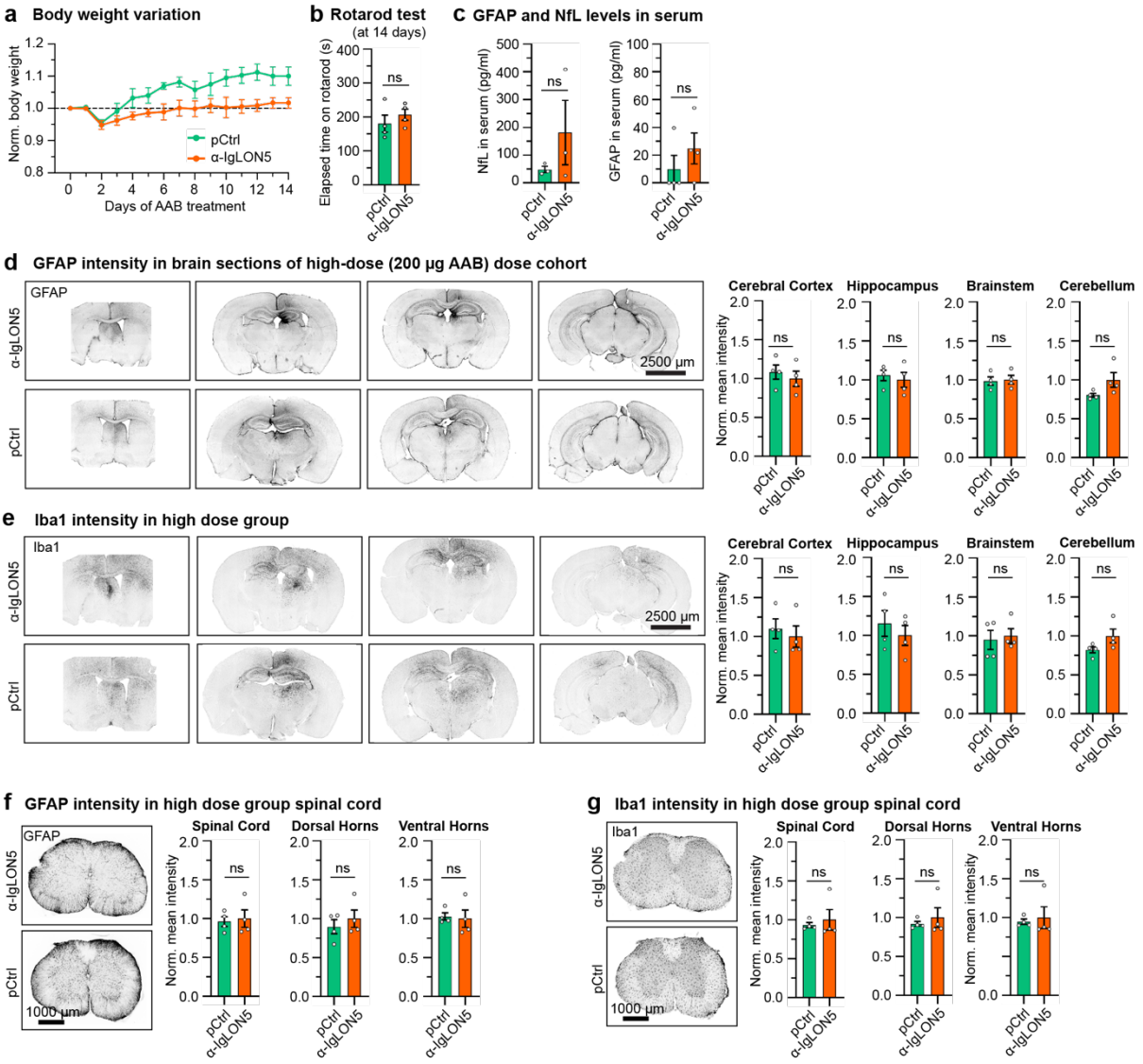

Supplementary Figure S4. **Changes observed upon infusion of high dose (200 µg AABs). a,** Body weight relative to Day 0 measured during 14 days of AAB treatment. Data shown as mean±SEM, N=4 animals per group. **d,** Rotarod performance (time spent on rod) of α-IgLON5 AAB and pCtrl animals determined at Day 14. Data shown as mean±SEM, N=4 animals per group. Student T-test. **c,** Serum levels of NfL and GFAP determined by ELISA. Data shown as mean±SEM, N=4 animals, with three technical replicates measured per animal. Student T-test**. d,** Representative coronal brain sections (anterior to posterior) immunolabeled for GFAP (astrocytes) and **e,** Iba1 (microglia) in α-IgLON5 AAB and pCtrl animals. Quantification of GFAP and Iba1 intensity in cerebral cortex, hippocampus, brainstem and cerebellum in α-IgLON5 AAB and control brains. Data shown as mean±SEM, N=4 animals, 3-5 brain sections per animal. Student T-test. **f,** Representative images, and quantification of GFAP and **g,** Iba1 immunolabeling in spinal cord sections. Data shown as mean±SEM, N=4 animals, 5-8 spinal cord sections per animal. Student T-test.

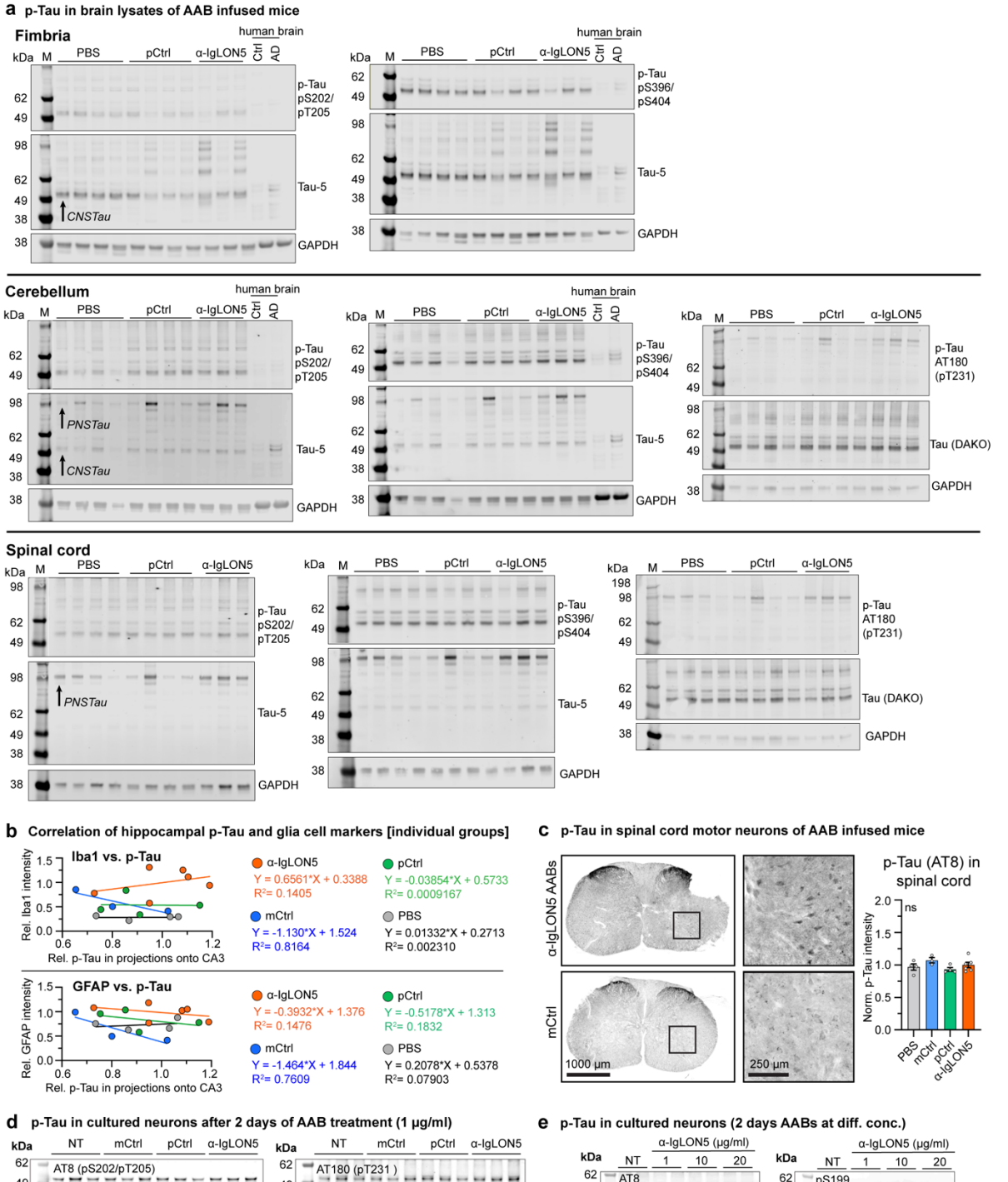
a p-Tau in brain lysates of AAB infused mice
Fimbria
Cerebellum
Spinal cord
human brain
kDa
M
PBS
pCtrl
α-IgLON5
Ctrl
AD
p-Tau pS202/pT205
p-Tau pS396/pS404
p-Tau AT180 (pT231)
Tau-5
Tau (DAKO)
GAPDH
CNSTau
PNSTau
b Correlation of hippocampal p-Tau and glia cell markers [individual groups]
Iba1 vs. p-Tau
Rel. Iba1 intensity
Rel. p-Tau in projections onto CA3
α-IgLON5
Y = 0.6561*X + 0.3388
R²= 0.1405
pCtrl
Y = -0.03854*X + 0.5733
R²= 0.0009167
mCtrl
Y = -1.130*X + 1.524
R²= 0.8164
PBS
Y = 0.01332*X + 0.2713
R²= 0.002310
GFAP vs. p-Tau
Rel. GFAP intensity
Y = -0.3932*X + 1.376
R²= 0.1476
Y = -0.5178*X + 1.313
R²= 0.1832
Y = -1.464*X + 1.844
R²= 0.7609
Y = 0.2078*X + 0.5378
R²= 0.07903
c p-Tau in spinal cord motor neurons of AAB infused mice
α-IgLON5 AABs
mCtrl
1000 µm
250 µm
p-Tau (AT8) in spinal cord
Norm. p-Tau intensity
ns
d p-Tau in cultured neurons after 2 days of AAB treatment (1 µg/ml)
NT
AT8 (pS202/pT205)
PHF-1 (pS396/pS404)
AT180 (pT231)
pS199
Total Tau
p-Tau norm. to total Tau
AT8
PHF-1
pS199
AT180
e p-Tau in cultured neurons (2 days AABs at diff. conc.)
α-IgLON5 (µg/ml)
AT8
PHF-1
pS199
pT231
Total Tau

965 **Supplementary Figure S5**. **p-Tau levels in brains and cultured neurons upon AAB treatment. a,**
966 Western Blot membranes probed for p-Tau (p-Tau pS202/pT205 (AT8), pS396/pS404 (PHF-1), and
967 pT231 (AT180) epitopes) and total Tau in lysates from fimbria, and cerebellum, and spinal cord tissues
968 of α-IgLON5 AAB and control animals. N=3-4 animals. Lysates from control and AD human brain were
969 included as controls. **b,** Correlation between normalized fluorescence intensities of hippocampal
970 microglia (Iba1, top) and astrocytes (GFAP, bottom) and p-Tau in projections onto CA3 for all treatment
971 groups, with linear fits for all individual control groups. A positive correlation only exists for Iba1 vs. p-
972 Tau in α-IgLON5 animals. **c,** Representative images of p-Tau (pS202/pT205 (AT8)) immunolabeling in
973 spinal cord sections of α-IgLON5 AAB and control mice, and quantification of mean intensity in the
974 spinal cord ventral horn. Data shown as mean±SEM, N=3-6 animals, 5-8 spinal cord sections per
975 animal. One-way ANOVA with Tukey post-test. **d**, Western Blot membranes probed for p-Tau (p-Tau
976 pS202/pT205 (AT8), pS396/pS404 (PHF-1), pS199 and pT231 (AT180) epitopes) and total Tau in
977 lysates from primary neurons treated with 1 μg/ml α-IgLON5 AABs and control antibodies for 2 days.
978 Two independent experiments with three technical replicates per treatment, data shown as mean±SEM.
979 One-way ANOVA with Tukey post-test. **e,** Western Blot membranes probed for p-Tau (p-Tau
980 pS202/pT205 (AT8), pS396/pS404 (PHF-1), pS199 and pT231 (AT180) epitopes) and total Tau in
981 lysates from cultured neurons treated with 1, 10 and 20 μg/μl α-IgLON5 AABs for 2 days. Two
982 independent experiment per treatment, data presented as mean±SEM. One-way ANOVA with Tukey
983 post-test.

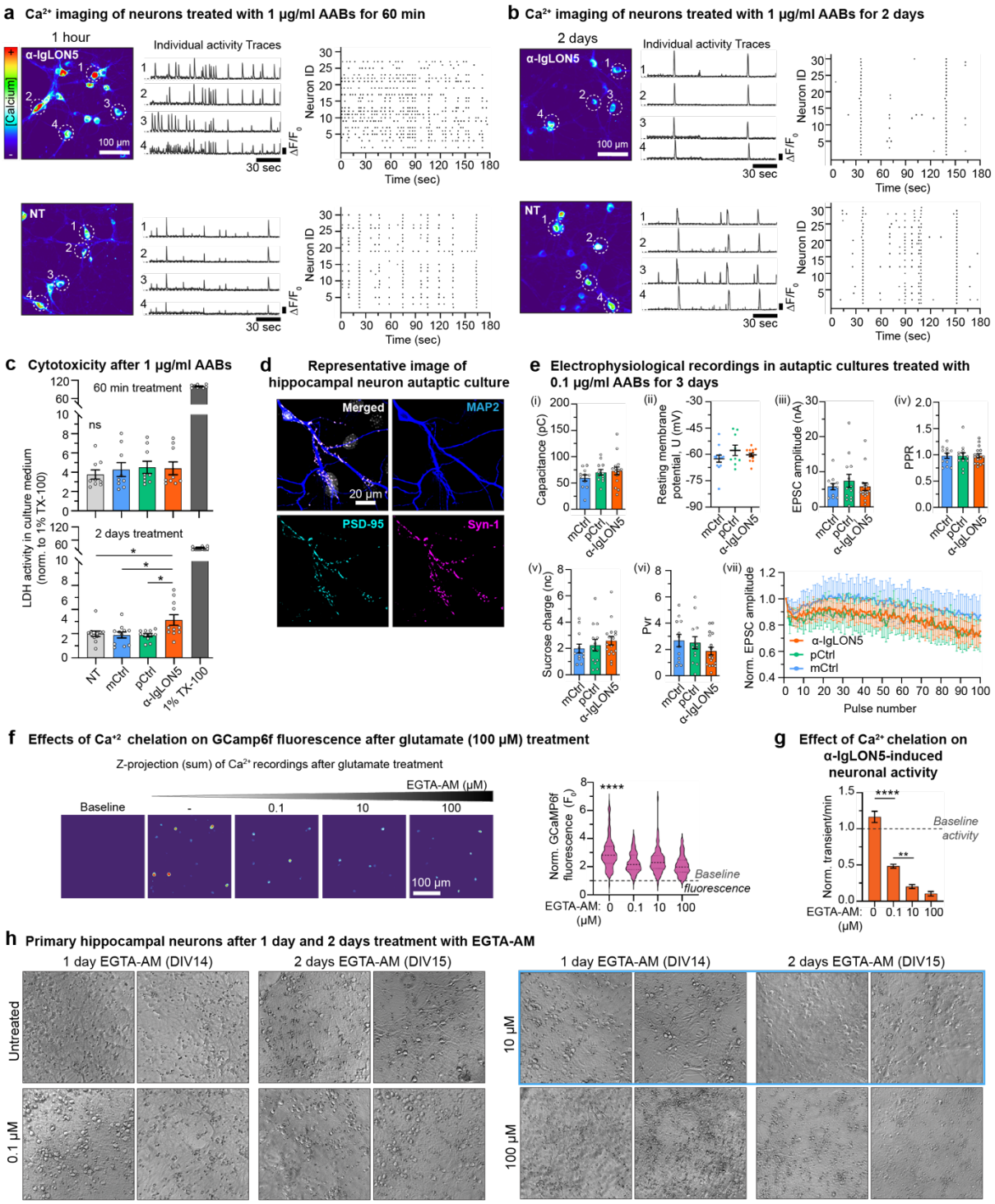

Supplementary Figure S6. α-IgLON5 AAB-induced acute neuronal hyperactivity and long-term silencing. a+b, Representative z-projection (sum) of Ca^{2+} recordings, individual activity traces, and raster plots for detected Ca^{2+} spikes after (**a**) 60 min and (**b**) 2 days exposure in neurons treated with 1 µg/ml α-IgLON5 or untreated (NT). **c,** LDH activity in culture media after 60 min and 2 days treatment with 1 µg/ml α-IgLON5 or control AABs. N=3 independent experiments with 3 technical replicates each, data presented as mean±SEM, One-way ANOVA with Tukey post-test **d,** Representative image of autaptic cultures immunolabeled for MAP2 (blue), PSD95 (cyan), Synapsin-1 (magenta) and DNA

993 (DAPI, white). **e,** Electrophysiological recordings in autaptic cultures treated with 0.1 μg/ml α-IgLON5
994 AABs and controls for 3 days. Measured parameters are (i) membrane capacitance (pC) and (i) resting
995 membrane potential, (iii) excitatory postsynaptic current (EPSC) amplitude, (iv) EPSC paired-pulse ratio
996 (PPR), (v) readily releasable pool size (sucrose charge), (vi) synaptic vesicle release probability (Pvr),
997 and (vii) EPSC release during 10 Hz stimulation. N=3 independent autaptic cultures. Data are presented
998 as mean±SEM, One-way ANOVA with Tukey post-test. **f,** Representative z-projection (sum) of Ca^{2+}
999 recordings and GCamp6f fluorescent intensity measurement in neurons treated with 100 μM glutamate
1000 for 30 min after 0.1, 10, 100 μM EGTA-AM treatment for 20 min. **g,** Frequency (transients/min) analysis
1001 in neurons pre-treated with 0.1, 10, or 100 μM EGTA-AM for 20 min and then exposed to 1 μg/ml α-
1002 IgLON5 or control AABs for 60 min. Data were collected from two primary neurons cultures and are
1003 shown as mean±SEM. One-way ANOVA with Tukey post-test. **h,** Primary neurons treated with 0.1, 10,
1004 or 100 μM EGTA-AM for 1 day and 2 days and imaged by bright field microscope.
1005
1006
1007
1008
1009
1010

1011 # Methods

1012 ***Ethics***

1013 All analyses of patient material were approved by the Charité - Universitätsmedizin Berlin
1014 Ethics Board (#EA1/258/18).
1015 Primary mouse neuron preparations and experiments involving adult animals (C57/B6, male)
1016 were carried out according to the guidelines stated in the directive 2010/63/EU of the
1017 European Parliament on the protection of animals used for scientific purposes and were
1018 approved by local authorities in Berlin and the animal welfare committee of the Charité
1019 university in Berlin, Germany.
1020

1021 ***Antibody Detection in patient CSF and serum.***

1022 Specificity of the purified α-IgLON5 AABs was confirmed by indirect immunofluorescence (IF)
1023 performed on HEK293 cells transfected with commercially available IgLON5 expression vector
1024 (EUROIMMUN, # 1151-1005-50) and cells with control transfection. α-IgLON5 AAB binding
1025 on cells was confirmed at dilutions of 1:100 for CSF and 1:1000 for serum.
1026

1027 ***Purification of patient-derived α-IgLON5 AABs***

1028 Recombinant human IgLON5-Fc chimera (R&D Systems) was bound to a 1 ml HiTrap® NHS-
1029 activated HP column (GE Healthcare) according to manufacturer's guide. For antibody
1030 isolation, eluates of plasmapheresis were loaded overnight onto the column. Then, the column
1031 was washed with 15 ml 20 mM Tris (pH 7.5) and 15 ml 0.5 M NaCl in 20 mM Tris (pH 7.5). α-
1032 IgLON5 AABs were eluted with 100 mM glycine (pH 2.2) with subsequent neutralization using
1033 1 M Tris (pH 8.8). Finally, the samples were re-buffered into phosphate-buffered saline (PBS)
1034 using Vivaspin® 15R ultrafiltration spin columns (Sartorius). For detection of specificity,
1035 recombinant IgLON5 or LG1 protein was spotted onto a nitrocellulose membrane (GE
1036 Healthcare), membranes were blocked with 1% BSA in PBS, incubated with α-IgLON5 AABs
1037 over night at 4°C, washed and incubated with HRP-coupled anti-human IgG. For detection of
1038 IgG subclasses, 2 μg of patient-derived AABs were dotted on a nitrocellulose membrane (GE
1039 Healthcare), membranes were probed with mouse anti-human IgG1-POD, anti-human IgG2-
1040 POD, anti-human IgG3-POD, and IgG4-POD ab (ThermoFisher Scientific), and sheep-anti-
1041 human IgG (Seramun).
1042 For the isolation of control serum IgGs (pCtrl), 750 μl serum from healthy controls were mixed
1043 with 450 μl protein A/G agarose (SantaCruz). IgG fractions were isolated according to
1044 manufacturer's instructions. Purity was checked by Coomassie staining. Protein concentration

1045 was determined using BCA protein assay Kit (ThermoFisher Scientific). The non-reactive
1046 human monoclonal control AAB (mCtrl; mGO53) was purchased from InVivoBiotech.
1047
1048 ***Relative binding strength quantification using flow cytometry***
1049 Binding strength was determined following previously published protocols [67]. In brief,
1050 HEK293T cells were transfected with cDNA plasmids coding for full human IgLON5 protein
1051 which co-expressed a myc-tag for transfection efficiency control. Three days post-transfection,
1052 cells were harvested and stained with serial dilutions of AABs and c-myc AABs. From live cells
1053 with top 30% protein expression (evaluated by c-myc signal), the mean fluorescence intensity
1054 (MFI) of Alexa488-coupled goat anti-human IgG (1:500; Life Technologies) was evaluated,
1055 and nonlinear regression models [$MFI=MFI_{max}$*IgG conc./ (0.5*MFI_{max} +IgG conc.)] under
1056 settings for one site specific binding were generated using GraphPad Prism 8 (GraphPad
1057 Software Inc.)
1058
1059 ***Tissue reactivity screening***
1060 Sagittal mouse brain sections were obtained from unfixed tissue, cut on a cryostat (Leica) at
1061 20 μm thickness and mounted on glass slides. Sections were rinsed with PBS, then blocked
1062 with PBS containing with 2% bovine serum albumin (BSA) and 5% normal goat serum (NGS)
1063 for 1 h at room temperature (RT), and incubated with α-IgLON5 AABs and pCtrl overnight at
1064 4°C. After three washes with PBS, goat anti-human IgG-AlexaFluor488 was applied for 2 h at
1065 RT, followed by staining with DAPI (1:1000 in PBS) for 5 min. Sections were washed with PBS
1066 before mounting with Immo-Mount (Epredia) and imaging using an inverted epifluorescence
1067 microscope (Leica SPE).
1068
1069 ***Epitope mapping in HEK293T cells expressing IgLON5 constructs***
1070 To map the epitopes of patient-derived α-IgLON5 AABs, we cloned human IgLON5 deletion
1071 constructs from full-length Myc-DKK-tagged human IgLON5 plasmid (Origene, #225495)
1072 using a Q5® Site-Directed Mutagenesis kit (New England Biolabs). Individual Ig domains of
1073 IgLON5 (Ig1, Ig2, and Ig3), or combinations thereof (Ig1+Ig2, Ig1+Ig3, and Ig2+Ig3), were
1074 expressed in HEK293T cells for 48 h. HEK293T cells were seeded on poly-L-lysine (PLL)
1075 coated coverslips and transiently transfected with either full-length IgLON5 or its deletional
1076 constructs. After fixation with 4 % paraformaldehyde (PFA) at RT for 10 min, blocking with 3%
1077 NGS in PBS for 1 h, cells were incubated with α-IgLON5 AABs or pCtrl overnight at 4°C. After
1078 washing and incubation with the AlexaFluor488-conjugated anti-human IgG for 1 h at RT.
1079 Binding of α-IgLON5 AABs was evaluated based on epifluorescence microscope (Leica SPE).
1080

1081 ***Antibody internalization experiments***

1082 α-IgLON5 AABs and pCtrl were conjugated with endosomal-pH sensitive red-fluorescent dye
1083 (pHrodo™ iFL Red STP ester, ThermoFisher Scientific) following the manufacturer's
1084 instructions. pHrodo™-conjugated antibodies were applied at 5 μg/ml to HEK293T cells
1085 overexpressing human full-length IgLON5 for 4 h at 37°C, or to primary mouse hippocampal
1086 neurons (DIV12) for 1 day or 2 days at 37°C. Images were captured on a spinning disc
1087 confocal microscope (Nikon, SoRa CSU-W1).

1088

1089 ***Intrathecal osmotic pump infusion***

1090 Eight weeks-old male C57Bl/6J wild-type mice were randomized for the different treatment
1091 groups by an independent investigator. α-IgLON5 AABs and non-reactive human monoclonal
1092 IgG (mCtrl) [21], IgG from healthy control individual serum (pCtrl), and PBS as controls - were
1093 delivered continuously into the right lateral ventricle over the course of 14 days, with a flow
1094 rate of 0.25 μl/h. Antibody cerebroventricular infusion was performed unilaterally using osmotic
1095 pumps (model 1002, Alzet, Cupertino, CA), which were loaded 24 h prior to surgical
1096 implantation. For pump implantation, mice were placed in a stereotaxic frame and a cannula
1097 was inserted into the right ventricle (Coordinates: 0.2 mm posterior and ± 1.00 mm lateral from
1098 bregma, depth 2.2 mm). The cannula was connected to a pump, which was subcutaneously
1099 implanted on the interscapular space of the animals. After surgery, mice were monitored daily
1100 to assess symptoms and body weight. Mice were sacrificed after 14 days and brain, spinal
1101 cord tissues, and serum were harvested.

1102 Two cohorts were infused with different amounts of antibodies: 1) Low dose cohort receiving
1103 75 μg antibody (~3 μg/g b.w.) consisted of α-IgLON5 (N=6), mCtrl (N=3), pCtrl (N=4), and
1104 PBS (N=4) animals. 2) High dose cohort receiving 200 μg antibody (8 μg/g b.w.) consisted of
1105 α-IgLON5 (N=4) and pCtrl (N=4) animals.

1106

1107 ***Tissue processing***

1108 For protein and RNA analysis, brain and spinal cord tissues were promptly dissected on ice,
1109 flash-frozen by placing on dry ice, and stored at -80°C until further use.

1110 <u>For protein extraction,</u> brain and spinal cord tissues were homogenized in ice-cold
1111 radioimmunoprecipitation assay (RIPA) buffer (Sigma-Aldrich) containing phosphatase and
1112 protease inhibitor cocktail (ThermoFisher Scientific) using a probe homogenizer. After
1113 incubating the homogenates on ice for 20 min, samples were centrifuged at 10000xg for 20
1114 min at 4°C and the protein concentration in supernatant was measured with BCA protein assay
1115 Kit (Pierce). Concentration of each sample was adjusted to 2 μg/μl and then mixed with 6 X

1116 SDS-containing Laemmli buffer (ThermoFisher Scientific). Subsequently, they were boiled at
1117 95 °C for 5 min and stored at -20°C until the Western blot analysis.
1118 For Immunohistochemistry (IHC), brain and spinal cord tissues were drop-fixed in 4% PFA for
1119 2 days. For cryoprotection, fixed tissues were sequentially transferred to 10%, 20% and 30%
1120 sucrose in PBS with 0.02% sodium azide at 4°C. Tissue was cut into 30 μm thick sections
1121 using cryostat (Leica) and serially collected in 50% glycerol in PBS to be stored at -20°C until
1122 used for IHC.
1123
1124 ***Western blot***
1125 To analyze total and p-Tau levels by Western blot, 10 μg of total protein per sample was
1126 loaded onto 4 to 12% bis-tris SDS- polyacrylamide gel (Invitrogen). Following electrophoresis,
1127 the separated proteins were transferred to a nitrocellulose membrane. The membrane was
1128 blocked with 3% BSA in PBS containing 0.05% of Tween (PBS-T) at RT for 1 h. Subsequently,
1129 the membranes were incubated with primary antibodies for total Tau, p-Tau and loading
1130 control, diluted in the blocking solution, overnight at 4°C. The following day, membranes were
1131 washed 3-times for 5 min in PBS-T and then incubated with fluorescent-dye conjugated
1132 secondary antibodies, diluted in blocking solution, for 1 h at RT. Membranes were then imaged
1133 using a Licor imaging system (Odyssey DLx). A full list of antibodies used in Western blot can
1134 be found in SupplementaryTable T2.
1135
1136 ***Histology***
1137 For immunodetection, 30 μm-thick PFA-fixed brain and spinal cord sections were washed free-
1138 floating in tris-buffered saline (TBS), permeabilized with 0.3% Triton X-100 in TBS for 20 min
1139 at RT, and washed 2-times for 5 min in TBS. All incubation steps were performed on an orbital
1140 shaker (180 rpm). Sections were blocked in blocking solution (3% NGS in TBS) for 1 h at RT.
1141 Sections were incubated with primary antibodies diluted in blocking solution at 4°C overnight.
1142 Next day, the sections were washed 3-times for 10 min in TBS and incubated with Alexa Fluor
1143 conjugated secondary antibody diluted in blocking solution for 2 h at RT. Sections were
1144 washed 3-times for 10 min in TBS and incubated with DAPI (1:1000 in PBS) for 15 min at RT.
1145 Sections were then mounted onto microscope slides and covered with coverslip using
1146 Fluoroshield™ mounting medium (Sigma-Aldrich). A full list of antibodies used IHC can be
1147 found in SupplementaryTable T2. Sections were imaged on a wide field fluorescence
1148 microscope (Eclipse-Ti, Nikon) using 10x objective with tiling function. Same imaging
1149 parameters were used while imaging the sections across different groups. Mean fluorescence
1150 intensity was measured using ImageJ from manually drawn regions of interest (ROIs) in the
1151 brain (on contralateral site to avoid injection confound) and spinal cord sections. Mean

1152 intensity was averaged over 3-5 sections for brain tissue or 5-8 sections for spinal cord tissue
1153 per animal.
1154 Detection of the spread of infused AABs was done in free-floating brain sections with goat
1155 anti-human HRP-conjugated secondary antibody in 3% NGS in TBS for 2 h at RT. Sections
1156 were washed 3-times for 5 min in TBS and the signal was amplified with a CF® 594 tyramide
1157 signal amplification kit (ThermoFisher Scientific).
1158
1159 ***Evaluation of serum***
1160 Levels of neurofilament light chain (NfL) and glial fibrillary acidic protein (GFAP) were
1161 measured from undiluted serum samples using commercial enzyme-linked immunosorbent
1162 (ELISA) kits according to manufacturer's instructions. (GFAP: Abbexa, NfL:Cloud-Clone).
1163
1164 ***RNA sequencing***
1165 RNA was extracted using High Pure RNA Tissue Kit (Roche) according to manufacturer's
1166 instructions. The quality of the purified total RNA was assessed with high sensitivity RNA
1167 screenTape with RIN number >7.0 and the RNA integrity was confirmed using Agilent
1168 Tapestation. Following ribosomal rRNA depletion, total RNAseq was sequenced in a paired
1169 end configuration using Illumina Novaseq 6000. Alignment and analysis scripts can be found
1170 at https://github.com/goldt/Iglon5_RNAseq. Computation has been performed on the HPC for
1171 Research cluster of the Berlin Institute of Health. Briefly, raw reads were aligned to GRCm39
1172 with STAR using gencode basic gene annotation (vM31) and the prepared
1173 GRCm39_Ensembl_rmsk_TE.gtf (Hammel laboratory). Count tables were generated using
1174 TEcount [68]. Upon investigation, sample IgG_2 (Animal 649) was found to have excessive
1175 gliosis and Iglon5_3 (Animal 660) had incomplete perfusion and were excluded from analysis.
1176 Differential expression was determined using the quasi-likelihood F test in edgeR by
1177 comparing Iglon5 treated vs PBS treated samples, and taking the top 250 differentially
1178 expressed genes using the TopTags function with corrected P values <0.05. Gene ontology
1179 (GO) enrichment analysis was performed using ShinyGO v0.77 (South Dakota State
1180 University, Brookings, SD, USA) to generate the list of pathways affected using gene ontology
1181 molecular function, cellular components and Kyoto Encyclopedia of Genes and Genomes
1182 (KEGG) databases.
1183
1184 ***Preparation of mouse primary neurons***
1185 Primary neurons were prepared from hippocampi dissected from P0-P1 wildtype mice of either
1186 sex. Hippocampi were dissected in ice-cold HBSS (Millipore) containing 1% P/S. Then,
1187 hippocampal tissue was digested in enzyme solution containing DMEM (ThermoFisher
1188 Scientific), (in mM) 3.3 cysteine, 2 CaCl2, 1 EDTA, and papain (20U/ml, Worthington) at 37°C

1189 for 30 min. Papain reaction was inhibited by incubating digested hippocampal tissue in DMEM
1190 containing 10% FBS (ThermoFisher Scientific), 1% P/S, 38 mM BSA, and 95 mM trypsin
1191 inhibitor at 37°C for 5 min. Cells then were triturated in complete Neurobasal-A (NBA) medium
1192 containing 10% FBS, 2% B-27, 1% Glutamax, 1% penicillin/streptomycin (P/S) and seeded in
1193 PLL (0.1 mg/mL) coated glass bottom μ-slide 8-well imaging dishes (ibidi) at a seeding density
1194 of ~30000 cells/cm^2 for IF experiments. For calcium (Ca^{2+}) imaging, neurons were seeded in
1195 96-well clear bottom black microplates (Corning) at a seeding density of 125000 cells/cm^2 and
1196 maintained at 37°C and 5% CO2 until used for experiments. After 3 h seeding the neurons,
1197 the media was completely changed to FBS and phenol-red free complete NBA medium. Every
1198 second day, one-fifth of the media was replaced by fresh complete NBA medium.
1199
1200 ***Differentiation of human neurons***
1201 Human neuronal stem cells (hNSCs) were differentiated using an inducible Neurog2 hNSCs
1202 through doxycycline induction. hNSCs were received from BIH Core Unit pluripotent Stem
1203 Cells and Organoids (CUSCO), Charité-Berlin. Cells were seeded in laminin 521 (Biolamina)-
1204 coated 8-well plates. The composition of the differentiation medium was: NBA, Neural
1205 Induction Supplement, Advanced DMEM/F12 (Gibco), supplemented by antibiotic (Gibco) and
1206 doxycycline (Sigma-Aldrich). On Day 4, the medium change was performed by the medium
1207 supplemented with AraC (Sigma-Aldrich), to reduce the number of non-neuronal cells. The
1208 differentiation medium was refreshed every day, the cells were cultivated for 43 days in 37°C
1209 and 5% CO_2.
1210
1211 ***IF in cultured neurons***
1212 Live staining (surface antigen binding): Primary mouse hippocampal neurons (DIV12) were
1213 treated with 1 μg/ml α-IgLON5 AABs or control antibodies and kept at 37°C and 5% CO_2 for
1214 60 min. Then, neurons were washed with PBS before fixation with 4% PFA in PBS for 15 min,
1215 and then washed with TBS for 10 min at RT. After fixation, neurons were blocked with 3%
1216 NGS for 1 h at RT and incubated with anti-human 488 secondary antibodies for 2 h at RT.
1217 After 3-times 10 min PBS washes, nuclei were stained with DAPI (1:1000 in PBS) for 10 min.
1218 Dishes were imaged with laser scanning confocal microscope (Nikon, A1Rsi+) with a x60 oil
1219 objective.
1220 Co-localization with synaptic markers: After the surface antigen labelling as described above,
1221 neurons were permeabilized with PBS containing 0.3% Triton X-100 for 20 min at RT. After
1222 two consecutive washing steps with excess PBS, neurons were blocked again with 3% NGS
1223 for 1 h. Neurons then were incubated with primary antibodies, diluted in blocking solution, for
1224 microtubule (MAP2) and pre- (Synapsin1), or post-(PSD95) synaptic markers overnight at

1225 4°C. Secondary and DAPI stainings were performed as described above. Dishes were imaged
1226 with laser scanning confocal microscope (Nikon, A1Rsi+) with a x60 oil objective using the z-
1227 stack function (z-step: 0,5 μm). Same imaging settings were used between each biological
1228 replicate (N=3) to allow the comparison for co-localization analysis which was performed using
1229 ImageJ.
1230 Tau missorting: Primary neurons were treated with different concentrations of α-IgLON5 AABs
1231 or control antibodies for either 2 days or 5 days. For Ca^{2+} depletion experiments, neurons
1232 were treated with 10 μM cell permeable Ca^{2+} chelator, EGTA-AM, (AAT Bioquest) 20 min prior
1233 to the antibody treatment. After the treatments, neurons were fixed at DIV9-12 with 4% PFA
1234 for 15 min and immunolabeled for total Tau and MAP2 by following the IF protocol described
1235 above. Antibody specifications are listed in SupplementaryTable T2. Neurons were imaged
1236 with spinning disc confocal microscope (Nikon, CSU-X), using 40X oil objective. Identical
1237 imaging settings were used between each biological replicate (N=3-4). Tau missorting
1238 analysis was done with ImageJ by calculating the mean intensity in somatodendritic
1239 compartment in Tau channel from manually drawn ROIs, as depicted in Fig. 4d.
1240 Cytotoxicy assay: Before fixing the cells, media was collected and centrifuged at 1400 rpm for
1241 1 min to remove the cell debris. A commercially available lactate dehydrogenase (LDH) kit
1242 was used to measure the release of LDH to the culture media (CyQUANT-ThermoFisher
1243 Scientific) according to the manufacturer's description.
1244
1245 ***Ca^{2+} imaging in cultured neurons***
1246 For Ca^{2+} imaging in cultured hippocampal neurons, AAV2/9 serotype was used for neuron
1247 specific expression of GCamp6f under *Syn* promoter. AAVs (ruby-P2A-GCamp6f) were
1248 ordered from Viral Core Facility of Charite Universitätsmedizin, Berlin (Catalog number: BA-
1249 026e). In cultured hippocampal neurons, 0.16 μl of 1,04 x 10^{13} v.g./ml of viruses were added
1250 to medium on DIV5. Ca^{2+} recordings were performed at DIV13-15.
1251 Ca^{2+} transient recordings: Neurons in 96-well plate expressing GCamp6f were recorded in a
1252 wide field fluorescence microscope (Eclipse-Ti, Nikon) with a 10x objective. Imaging dishes
1253 were placed in the live-cell imaging chamber of the microscope to maintain an environment of
1254 37°C, 5% CO_2 and ~95% humidity. α-IgLON5 AABs or control antibodies were added to the
1255 wells by direct application. Ca^{2+} imaging was done in the green channel and mRuby
1256 expressing neurons were visualized in the red channel. Ca^{2+} transients were recorded for 180
1257 sec at ~8 Hz. Two to three wells in three independent cultures were analyzed per condition.
1258 Analysis: ROIs were created for each soma in red channel using a custom written script in
1259 Cell Profiler. Created ROIs were placed over each frame of the video recorded in green
1260 channel and mean intensity over time was measured using ImageJ. The .csv files containing

1261 mean fluorescent intensity from each image of the time-lapse videos were processed using
1262 the FluoroSNNAP application for ΔF/F0 conversion and spike detection [69]. In short, .csv files
1263 were uploaded to FluoroSNNAP and the function "Convert raw fluorescence data to ΔF/F0"
1264 was used to compute baseline fluorescent by taking the average of 50th percentile of the
1265 signal across a 60 s time window. Ca^{2+} transients from individual ROIs were detected with a
1266 template-based approach. This method identifies events by comparing a moving window of
1267 the Ca^{2+} signal to a predefined library of Ca^{2+} waveform templates. Events were detected with
1268 a similarity threshold of 0.75 and a minimum amplitude of 0.01. Hyperactivity criteria was
1269 calculated for each time point independently by taking the mean±SD of pCtrl group as a
1270 reference value for normal activity: Spike frequencies larger than [mean+2*SD] of pCtrl were
1271 considered as hyperactivity.
1272
1273 ***Electrophysiology in primary autaptic cultures***
1274 Isolated primary neurons on micro islands of glial cells ("autaptic cultures") were prepared
1275 from wildtype mice as recently described [70], with slight modifications. Briefly, 300 µm spots of
1276 a growth-permissive substrate mix of 0.7 mg/ml collagen and 0.1 mg/ml poly-D-lysine were
1277 printed on glass coverslips coated with agarose. Astrocytes were seeded onto these
1278 coverslips in DMEM (ThermoFisher Scientific), supplemented with 10% fetal calf serum and
1279 0.2% P/S (Invitrogen). After formation of glia micro-islands, DMEM was replaced with NBA
1280 supplemented with 2% B27 and 0.2% P/S. Hippocampal neurons prepared from P0 mice were
1281 added at a density of 370 cells/cm^2. Prior to electrophysiological recordings, autaptic cultures
1282 were treated with antibodies at a final concentration of 0.1 µg/ml for 3 days.
1283 Electrophysiological recordings: Neurons were recorded at DIV13-17 at RT on an IX73
1284 inverted microscope (Olympus) using a Multiclamp 700B amplifier under the control of a
1285 Digidata 1550 AD board and Clampex 10 software (all Molecular Devices). Data were acquired
1286 at 10 kHz and filtered at 3 kHz, and series resistance was compensated at 70%. The
1287 extracellular solution contained (in mM) 140 NaCl, 2.4 KCl, 10 HEPES, 10 glucose, 2 $CaCl_2$,
1288 and 4 $MgCl_2$ (pH adjusted to 7.3 with NaOH, 300 mOsm). The intracellular solution contained
1289 (in mM) 136 KCl, 17.8 HEPES, 1 EGTA, 4.6 $MgCl_2$, 4 Na_2ATP, 0.3 NaGTP, 12 disodium
1290 phosphocreatine, 50 U/ml creatine phosphokinase, pH adjusted to 7.3 with KOH, 300 mOsm.
1291 Autaptic neurons were recorded in whole-cell voltage clamp mode using thick-walled
1292 borosilicate pipettes with a tip resistance of 3-4 MΩ. Membrane potential was set to −70 mV.
1293 Paired EPSCs were evoked every 5 s by triggering two unclamped action potentials with 40
1294 ms interstimulus interval using 1 ms depolarizations of the soma to 0 mV. The readily-
1295 releasable pool of synaptic vesicles was determined by application of a hypertonic 500 mM
1296 sucrose solution for 10 sec. Electrophysiological recordings were analyzed using AxoGraph.

The vesicular release probability was calculated as the ration of the charge of the sucrose evoked response by the average charge of six EPSCs prior to the sucrose application. The paired-pulse ratio was calculated as the ratio from the second and first EPSC amplitude.

Statistical analysis

All data plotting and statistical analyses were performed in GraphPad Prism 9. Comparison of two groups was done by Student T-test and multiple group comparisons were performed by one-way ANOVA with Tukey or Holmes-Sidak, or as indicated in the figure legends. ****$p < 0.0001$, ***$p < 0.001$, **$p < 0.01$, *$p < 0.05$.

Data and code availability

Lists of differentially expressed gene can be found in Supplementary Table T1. Scripts for RNAseq analysis can be found at https://github.com/qoldt/Iglon5_RNAseq and the used code is provided at file:///Users/wegmanns/Downloads/IgLON5_code%20for%20RNAseq%20analysis.html.